Univerzita Karlova v Praze

Matematicko-fyzikální fakulta

DIPLOMOVÁ PRÁCE

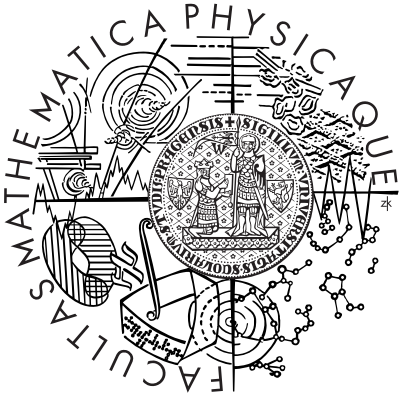

Vojtěch Krejčiřík

Produkce hyperjader v reakcích záchytu kaonu K^-

Ústav teoretické fyziky

Vedoucí diplomové práce: RNDr. Aleš Cieplý, CSc.,
Ústav jaderné fyziky, AVČR, v. v. i.

Studijní program: Fyzika, Teoretická fyzika

2009

Charles University in Prague

Faculty of Mathematics and Physics

DIPLOMA THESIS

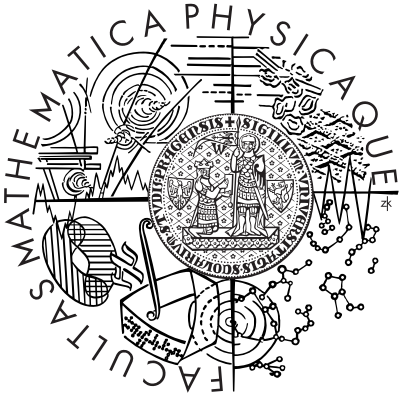

Vojtěch Krejčiřík

Hypernuclear production in K^- stopped reactions

Institute of Theoretical Physics

Supervisor: RNDr. Aleš Cieplý, CSc.,

Nuclear Physics Institute, ASCR

Study program: Physics, Theoretical physics

2009

I would like to express gratitude to my supervisor Aleš Cieplý for his guidance, patience and hours of valuable discussions. I also thank Jiří Mareš and other members of our group for plenty of advices and friendly atmosphere they create.

I am also very grateful to my parents and Anička for their endless love and encouragement. I would never accomplish this work without them.

This work was supported by the GAUK grant 91509.

I declare that I wrote the diploma thesis by myself and I used solely adduced references. I agree with lending of this work.

Prohlašuji, že jsem svou diplomovou práci napsal samostatně a výhradně s použitím citovaných pramenů. Souhlasím se zapůjčováním práce a s jejím zveřejňováním.

In Prague 14.4.2009 Vojtěch Krejčiřík

Contents

Název práce: Produkce hyperjader v reakcích záchytu kaonu K^-

Autor: Vojtěch Krejčiřík

Katedra (ústav): Ústav teoretické fyziky

Vedoucí diplomové práce: RNDr. Aleš Cieplý, CSc.,
Ústav jaderné fyziky, AVČR, v. v. i.

E-mail vedoucího: cieply@ujf.cas.cz

Abstrakt:

Předkládaná diplomová práce se zabývá studiem produkce Λ-hyperjader v reakcích způsobených kaonem K^- zachyceným na atomové orbitě. Výpočty jsou provedeny v rámci impulsové aproximace s porušenými vlnami (DWIA). Elementární proces kaon-nukleon popisujeme pomocí mikroskopického modelu založeného na chirální poruchové teorii. Použití mikroskopického modelu je jedním z přínosů práce. Jako první navíc zahrnujeme efekt pionové distorze při výpočtu efektivní nukleonové hustoty dostupné pro reakci. V samotných výpočtech uvažujeme několik kaon-jaderných i pion-jaderných potenciálů. Studujeme vliv různých faktorů na výslednou pravděpodobnost reakce. Naše závěry porovnáváme s experimentálními daty a předchozími teoretickými pracemi na toto téma. Ačkoli jsou naše výsledky bliže k experimentálně naměřeným hodnotám než výsledky předchozích autorů, shoda s experimentem stále není plně uspokojivá.

Klíčová slova: hyperjádro, K^- meson, DWIA aproximace, optický potenciál

Title: Hypernuclear production in K^- stopped reactions

Author: Vojtěch Krejčiřík

Department: Institute of theoretical physics

Supervisor: doc. RNDr. Aleš Cieplý, CSc.,
Nuclear Physics Institute, ASCR

Supervisor's e-mail address: cieply@ujf.cas.cz

Abstract:

The thesis focuses on Λ-hypernuclear production induced by K^- meson stopped at an atomic orbit. Calculations are performed within the framework of the distorted wave impulse approximation. We use a microscopic model based on chiral perturbation theory for the description of the elementary kaon-nucleon process. The use of the microscopic model is one of the assets of the present work. Another novelty is a proper treatment of the pion distortion in the effective nucleon density available for the reaction. We consider several kaon-nucleus and pion-nucleus potentials. We study various effects on the capture rate of the reaction. We compare our results with experimental data and with previous calculations. Although our results are closer to the experimental values then the results of previous authors, the agreement with experiment is still unsatisfactory.

Keywords: hypernucleus, K^- meson, DWIA approximation, optical potential

Chapter 1

Introduction

A hypernucleus is a bound system of nucleons (protons, neutrons) and at least one hyperon (Λ, Σ, Ξ, ...). The first hypernucleus was detected in an interaction of cosmic rays with emulsion in 1952 [1] and totally 37 Λ-hypernuclei [2] and 4 double Λ-hypernuclei [3] have been observed since then.

A hyperon is distinguishable from a nucleon, therefore its behaviour in the nuclear medium is not affected by the Pauli exclusion principle. This makes the hyperon an ideal and unique probe of the deep nuclear interior. The added hyperon introduces a new dimension to the traditional nuclear physics dealing with nuclei composed only of protons and neutrons. It represents the first step to a more general world of flavoured nuclei. Hypernuclei enable us to study various nuclear models as well as models of baryon-baryon or meson-baryon interaction in the strange sector. Strange particles (hyperons and possibly kaons) are also expected to play an important role in neutron stars [4] and the study of hypernuclei can provide valuable information about the properties of matter under such extreme conditions. Weak decays of hyperons bound in hypernuclei also provide a tool for investigation of the propagation of pions in the nuclear medium in addition to the study of weak interaction.

Hypernuclei can be produced in various reactions. For example, the elementary

process can be the conversion of a nucleon N into a hyperon Y in the reaction

$$a + N \rightarrow b + Y \ , \quad N(a,b)Y.$$

Systematical experimental studies of hypernuclei began in the early 70s. Experiments using kaon beams in CERN (Switzerland) and later in BNL (USA) and FINUDA (Italy) enabled physicists to explore hypernuclei produced in (K^-, π) reactions [5, 6, 7, 8]. The study of (π^+, K^+) reactions started in the mid 80s in BNL [9] and proceeded intensively in KEK (Japan) [10, 11]. The first successful measurement of $(e, e'K^+)$ reaction took place at JLab (USA) in 2003 [12].

The study of strangeness exchange reactions induced by kaon (stopped or in flight) can provide additional information about the K^--nucleus interaction. For example, one can study the effect of the depth of the kaon-nucleus potential on the calculated characteristics of the hypernuclear production processes. The depth of the kaon-nucleus potential is still an open question. On one hand, fits to K^--atomic data based on phenomenological density dependent optical potentials [13, 14] or on the relativistic mean field theory [15, 16] lead to kaon-nucleus potential of depth $150 - 200$ MeV. On the other hand, calculations using chiral models fitted to K^-N scattering and K^--atomic data result in potentials of depth $50 - 100$ MeV [17, 18]. The depth of the K^--nucleus potential is closely related to possible existence of deeply bound $\bar{K}$-nuclear states or the question of kaon condensation The analysis of hypernuclear production might help to answer the question about the depth of K^--nucleus potential.

The reaction we focus on in this work is the Λ-hypernuclear production induced by the stopped kaon, $(K^-_{\text{stopped}}, \pi)$. In this type of reaction, the kaon is slowed down and then captured at an atomic orbit. Then it cascades down to a lower orbit and finally is absorbed by the nucleus. One of the nucleons changes to the Λ-hyperon and the created pion escapes away. The first observation of this reaction took place in CERN in 1973 [5] and most recent experimental data come form KEK [19], FINUDA [8] and BNL [20]. The (K^-, π^-) was measured in KEK in the 80s and is measured in FINUDA nowadays.

Only the production preserving nuclear charge (e.g. ^{12}C $\rightarrow$ $^{12}_{\Lambda}$C) is accessible in this kind of measurement. In BNL, the (K^-, π^0) reaction was measured via the detection of photons produced in the decay of the outgoing neutral pion. This method makes it possible to study processes with change of the nuclear charge (e.g. ^{12}C $\rightarrow$ $^{12}_{\Lambda}$B). Several theoretical attempts to describe the $(K^-_{\mathrm{stopped}}, \pi)$ hypernuclear productions have been made [18, 21, 22], but none of them led to satisfactory predictions. The calculated capture rates were at least three times smaller then the experimental values.

In this work, we focus on target nuclei ^{12}C and ^{16}O and consider all possible produced Λ-hypernuclei: $^{12}_{\Lambda}$C, $^{12}_{\Lambda}$B, $^{16}_{\Lambda}$O, $^{16}_{\Lambda}$N. The terminology used in hypernuclear physics is as follows: The hypernucleus $^{12}_{\Lambda}$C consists of 12 baryons and one of them is the Λ hyperon. Its atomic number is 6, as denoted by the label C (in general, the atomic number is equal to the charge of the system, not necessarily to the number of protons). The hypernucleus $^{12}_{\Lambda}$C thus contains six protons, five neutrons and one Λ hyperon.

We use the distorted wave impulse approximation (DWIA) as a theoretical framework for the description of the hypernuclear production. This approach describes a target nucleus as a collection of individual particles and assumes that the reaction with the kaon proceeds on one of those particles. The other particles are regarded as spectators and contribute only to the environment, in which the interaction takes place. Together with the interacting baryon, they generate an optical potential, by which the incident and outgoing particles are distorted. The nuclear medium also affects the elementary kaon-nucleon process. To summarize, the primary many-body problem (kaon-nucleus) is replaced by the two-body problem (kaon-nucleon) and the distortions of incident and outgoing wave functions caused by the relevant optical potential.

We consider several optical potentials (deep as well as shallow) for the distortion of the kaon in the initial state and also for the distortion of the pion in the final state. We study and discuss effects related to the different choices of optical potentials.

We describe the elementary kaon-nucleon process within the framework of the mi-

croscopic model based on the chiral Lagrangian, whereas previous authors [18, 21, 22] used elementary branching ratios ambiguously derived from experiments. We consider both the experimental values as well as the microscopically calculated branching ratios and compare the results.

Our microscopic model of the elementary process is based on the chiral perturbation theory of meson-baryon interactions [17, 18, 23, 24, 25, 26]. It is an effective theory [27, 28] that implements the symmetries of quantum chromodynamics (QCD) in the low energy region, where the direct use of QCD is problematic due to its nonperturbative character. The hypernuclear physics is one of the areas, where the predictions of the chiral perturbation theory can be tested.

The DWIA formalism and the microscopic model for elementary reactions are outlined in Chapter 2. In Chapter 3, we present the input wave functions we use. The results of numerical calculations are presented and discussed in Chapter 4. In Chapter 5, we summarize our work and present the outlook for the future.

Chapter 2

Formalism

In this chapter, we outline the basic ideas of the distorted wave impulse approximation (DWIA) and use this approach to in the study of the hypernuclear production induced by stopped kaon. The replacement of the many-body problem by the two-body problem, which is the basic idea standing behind the DWIA, requires the description of the elementary two-body process. The model of the elementary process is given in the first section. The DWIA is applied to the hypernuclear production in the second section.

The hypernuclear production in K^- stopped reaction can be written as a reaction

$$K^- + \mathrm{A} \rightarrow \pi + \mathrm{H}. \tag{2.1}$$

The initial state is a K^--atomic bound state with a nucleus A and the final state is an outgoing pion with a hypernucleus H. The reaction is illustrated in figure 1.

The reaction of a kaon with a nucleus is a complicated many-body problem, which cannot be described in all its complexity, therefore we have to look for a simplification. One may consider the nucleus as a collection of individual particles and assume that the reaction occurs on one of them, while the other nucleons are regarded as spectators and contribute to the environment, in which the process takes place.

The many-body problem of the reaction of a kaon with an entire nucleus is thus replaced by the two-body reaction of the kaon with one nucleon. We call it an elementary

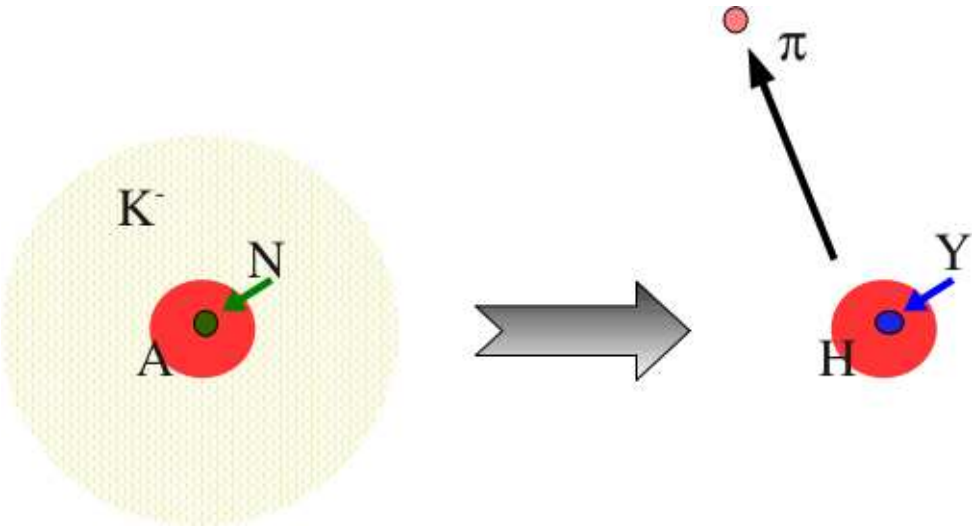

Figure 1: A schematic draft of the A($K^-_{\text{stopped}}, \pi$)H reaction.

or one-baryon process. Since the kaon in the initial state and the pion in the final state are affected by the interaction with the nucleus, we cannot use the wave functions of free particles. The effect of the nucleus on the kaon and pion wave functions is described by an optical potential. We say that the wave functions are distorted. An important factor is the overlap of the wave functions of kaon and pion and the nuclear to hypernuclear transition density.

This approach is called the distorted wave impulse approximation (DWIA). For technical details, we refer the reader to special monographs, e.g. [29, 30].

2.1 Elementary process

Our approach, which is based on the DWIA, requires the knowledge of an elementary process, the reaction of a kaon with a nucleon

$$K^- + N \to \pi + Y. \tag{2.2}$$

Though one can get the necessary information from experiment, we decided to use a microscopic model.

The starting point of our model is the chiral perturbation theory and its Lagrangian density. We do not intend to develop the formalism of renormalized quantum field theory and sum contributions of all loop Feynman diagrams, therefore we use the approach of effective potentials, which is more useful for our purposes. They can be used in a the Lippmann-Schwinger equation (known from the quantum scattering theory) to obtain t-matrix elements, which already contain the essential information about the pertinent process. Since the elementary process takes place in the nuclear medium, the situation is different from that in the vacuum. We consider the effect of Pauli blocking in the intermediate states as a first step to a more complex description of the in-medium reaction.

2.1.1 Chiral Lagrangian density

The reaction of a kaon with a nucleon belongs to a more general set of meson-baryon reactions. Following references [23, 24], we describe meson-baryon interactions in the formalism of the quantum field theory by the chiral Lagrangian density. The leading order term is given by

$$\begin{aligned} \mathcal{L}^{(1)} &= \mathrm{Tr}\left(\overline{\Psi}_B \left(i\gamma_\mu D^\mu - M_0\right)\right) + F\,\mathrm{Tr}\left(\overline{\Psi}_B \gamma_\mu \gamma_5 \left[A^\mu, \Psi_B\right]\right) \\ &\quad + D\,\mathrm{Tr}\left(\overline{\Psi}_B \gamma_\mu \gamma_5 \left\{A^\mu, \Psi_B\right\}\right). \end{aligned} \tag{2.3}$$

The covariant derivative is defined as

$$D^\mu \Psi_B = \partial^\mu \Psi_B + \left[\Gamma^\mu, \Psi_B\right], \tag{2.4}$$

where

$$\Gamma^\mu = \frac{1}{8f_0^2}\left[\phi, \partial^\mu \phi\right] + O(\phi^4). \tag{2.5}$$

Here f_0 is the pseudoscalar meson decay constant, M_0 is the baryon mass in the chiral limit, and D and F are the vector and axial vector coupling constants. The matrix Ψ_B stands for the octet of baryon Dirac fields

$$B = \begin{pmatrix} \frac{\Lambda}{\sqrt{6}} + \frac{\Sigma^0}{\sqrt{2}} & \Sigma^+ & p \\ \Sigma^- & \frac{\Lambda}{\sqrt{6}} - \frac{\Sigma^0}{\sqrt{2}} & n \\ \Xi^- & \Xi^0 & -\frac{2}{\sqrt{6}}\Lambda \end{pmatrix}, \tag{2.6}$$

and ϕ for the octet of pseudoscalar meson fields

$$\phi = \begin{pmatrix} \frac{\eta_8}{\sqrt{6}} + \frac{\pi^0}{\sqrt{2}} & \pi^+ & K^+ \\ \pi^- & \frac{\eta_8}{\sqrt{6}} - \frac{\pi^0}{\sqrt{2}} & K^0 \\ K^- & \overline{K^0} & -\frac{2}{\sqrt{6}}\eta_8 \end{pmatrix}. \tag{2.7}$$

2.1.2 Potential model

We intend to establish the formalism of effective potentials and not to work in a framework of quantum field theory. The connection between the two formalisms is achieved by the requirement of equal s-wave scattering lengths calculated up to order q^2. The second order chiral Lagrangian density $\mathcal{L}^{(2)}$ contributes to the order q^2 too, but we do not specify it here. We refer the reader to [23, 25] for the details.

We take the potentials in the separable form [23]

$$V_{ij}(k_i, k_j) = \frac{C_{ij}}{4\pi^2 f_0^2} \sqrt{\frac{M_i M_j}{s\omega_i\omega_j}} \frac{\alpha_i^2}{\alpha_i^2 + k_i^2} \frac{\alpha_j^2}{\alpha_j^2 + k_j^2}\,. \tag{2.8}$$

The advantage of the separable form of the potential is that many calculations can be performed analytically. Coefficients C_{ij} are determined directly by the chiral Lagrangian structure, ω_l $(l = i, j)$ is the reduced energy in the lth channel, s is the total c.m. energy, M_l is the baryon mass, k_l is the c.m. momentum, and α_l is the inverse range parameter for channel l.

The Lippmann-Schwinger equation for coupled channels reads

$$t_{ij}(k_i, k_j) = V_{ij}(k_i, k_j) + \sum_{n=1}^{N} \frac{\omega_n}{2\pi} \int \mathrm{d}^3 l\, \frac{V_{in}(k_i, l) t_{nj}(l, k_j)}{k_n^2 - l^2 + i\epsilon}, \tag{2.9}$$

where N is the number of considered channels.

Coupled channels considered in one specific calculation are determined by laws of conservation of charge, strangeness and baryon number [24]. For example, if we look for an amplitude of an elementary reaction of the meson K^- with the proton ($Q = 0$, $S = 1$, $B = 1$), the channels one has to consider in the LS equation are: $\pi^0\Lambda$, $\pi^0\Sigma^0$, $\pi^-\Sigma^+$, $\pi^+\Sigma^-$, K^-p, $\bar{K}^0n$, $\eta\Lambda$, $\eta\Sigma^0$, $K^0\Xi^0$, $K^+\Xi^-$. The amplitude for the reaction of the kaon with the neutron, which is also needed, can be obtained either by a different choice of coupled channels or by using the assumption of isospin symmetry.

2.1.3 Pauli blocking

The elementary process takes place in the nuclear medium. A medium effect, which can be easily taken into account, is the Pauli exclusion principle in the intermediate states [17].

If we denote the momentum of a target nucleon in the laboratory frame $\mathbf{p}$, the relative K^-N momentum in the intermediate state (the integration variable in LS equation) $\mathbf{l}$ and in the initial state k_j. The momentum of the nucleon in the intermediate state in the laboratory frame is $\mathbf{p'} = \mathbf{p} + \mathbf{k_j} - \mathbf{l}$. The Pauli principle requires that the momentum $\mathbf{p'}$ must be greater than the Fermi momentum. This restriction changes the domain of integration in the Lippmann-Schwinger equation (2.9) to Ω_n

$$\Omega_n(p_F) = \{\mathbf{l}\,;\ |\mathbf{p} + \mathbf{k_j} - \mathbf{l}| \geq p_F\}\,.$$

The Pauli exclusion principle relates only to systems of identical fermions, therefore the change of integration domain is applied only to the channels with protons or neutrons, while the integration domain in other channels is not altered.

The separable form of potentials allows us to write them as

$$V_{ij} = v_{ij} g_i(k_i) g_j(k_j),$$

where v_{ij} is practically independent of momenta and $g_l(k_l)$ is the Yamaguchi form factor

$$g_l(k_l) = \frac{\alpha_l^2}{\alpha_l^2 + k_l^2}\,.$$

The t-matrix has the same form

$$t_{ij}(k_i, k_j) = t^0_{ij} g_i(k_i) g_j(k_j). \tag{2.10}$$

If we put these expressions in the Lippmann-Schwinger equation (2.9), we obtain the result for t^0_{ij} in a purely algebraic form,

$$t^0_{ij} = v_{ij} + \sum_n v_{in}\, I_n\, t_{in}, \tag{2.11}$$

where the relevant integral is

$$I_n = \frac{\omega_n}{2\pi} \int_{\Omega_n(p_F)} \mathrm{d}^3 l\, \frac{1}{k_n^2 - l^2 + i\epsilon} \frac{\alpha_n^2}{\alpha_n^2 + l^2}. \tag{2.12}$$

This integral can be solved analytically ($\kappa = |\mathbf{k_j} + \mathbf{p}|$)

$$\begin{aligned} I_n(\kappa, k_n, p_F) \;=\; & \omega_n \left(\frac{\alpha_n^2}{\alpha_n^2 + k_n^2}\right)^2 \left[\frac{k_n^2 - \alpha_n^2}{2\alpha_n} \left(\operatorname{arccot}\frac{p_F - \kappa}{\alpha_n} + \operatorname{arccot}\frac{p_F + \kappa}{\alpha_n}\right)\right. \\ & -\frac{1}{4\kappa}\left(p_F^2 - \kappa^2 - k_n^2\right) \ln \frac{\alpha_n^2 + (p_F + \kappa)^2}{\alpha_n^2 + (p_F - \kappa)^2} \\ & -\frac{1}{4\kappa}\left((k_n + \kappa)^2 - p_F^2\right) \ln \frac{|p_F + k_n + \kappa|}{|p_F - k_n - \kappa|} \\ & \left.-\frac{1}{4\kappa}\left((k_n - \kappa)^2 - p_F^2\right) \ln \frac{|p_F - k_n + \kappa|}{|p_F + k_n - \kappa|}\right]. \end{aligned} \tag{2.13}$$

The evaluation of the integral is given in Appendix A. It is obvious, that the integral for the intermediate channel without a nucleon is obtained by setting $p_F = 0$. The limit $p_F = 0$ and $\mathbf{p} = \mathbf{0}$ corresponds to the free space t-matrix. The solution of the equation (2.11) together with the ansatz (2.10) gives us required t-matrix elements.

2.2 Hypernuclear production

We follow ref. [21] and assume the T-matrix for the reaction of a kaon with a nucleus in the form

$$T_{if}(\mathbf{q_f}) = t_{if}(\mathbf{q_f}) \int \mathrm{d}^3\mathbf{r}\ \chi^*_{q_f}(\mathbf{r})\ \rho_{if}(\mathbf{r})\ \Psi_{NLM}(\mathbf{r})\ . \tag{2.14}$$

Here, $t_{if}(\mathbf{q_f})$ denotes the t-matrix element for the elementary process, $\Psi_{NLM}(\mathbf{r})$ is the K^- wave function distorted by a K^--nucleus optical potential, $\chi^*_{q_f}(\mathbf{r})$ is the wave function of the outgoing pion distorted by a pion-nucleus optical potential, $\mathbf{q_f}$ is the momentum of the outgoing pion. The nucleus to hypernucleus transition density matrix reads

$$\rho_{if} = \left\langle H \left| \sum_{\alpha\beta} \psi^{Y*}_{\beta}(\mathbf{r}) \psi^{N}_{\alpha}(\mathbf{r}) a^{+}_{Y}(\beta) a_N(\alpha) \right| A \right\rangle ,$$

where α, β run over all single particle states of nucleons in the nucleus (α) and hyperons in the hypernucleus (β), respectively.

The capture rate for reaction (2.1) is given by

$$\begin{aligned} \Gamma_{if} &= 2\pi \int \delta(E_\pi + E_H - E_{K^-} - E_A)\ \left\langle |T_{if}(\mathbf{q_f})|^2 \right\rangle\ \frac{d^3q_f}{(2\pi)^3} \\ &= \frac{1}{(2\pi)^2}\, q_f \omega_f \int < |T_{if}(\mathbf{q_f})|^2 >\ d\Omega_{q_f}, \end{aligned} \tag{2.15}$$

where we use spherical coordinates and the delta-function to integrate over the magnitude of q_f. The brackets $< \cdots >$ are used to denote that the square of the T-matrix is averaged over initial states and summed over all final states. The reduced energy in the final state is denoted by ω_f and reads

$$\omega_f{}^{-1} = E_\pi{}^{-1} + E_H{}^{-1}.$$

Before we proceed, we focus on the kinematics of the elementary process. The situation is complicated by the fact, that the elementary process takes place in the nuclear medium. The capture rate for the elementary process $\overline{\gamma}(K^-N \to \pi Y)$ is connected with

the t-matrix element, which enters eq. (2.14) by the relation

$$\overline{\gamma}(K^- N \to \pi Y) = \frac{\overline{q}_f \overline{\omega}_f}{\pi} \mid t_{if}(\overline{q}_f) \mid^2, \tag{2.16}$$

where the bar indicates that the quantities are considered in the nuclear medium. Because we don't know the particular nucleon, on which the reaction takes place, the quantities are averaged due to the Fermi motion of nucleons within the nuclear medium. Applying relations (2.14) and (2.16) in the formula for the capture rate (2.15) yields

$$\Gamma_{if} = \frac{q_f \omega_f}{\overline{q}_f \overline{\omega}_f} \, \overline{\gamma}(K^- N \to \pi \Lambda) \int \left\langle \left| \int \mathrm{d}^3 r \; \chi^{(-)^*}_{q_f}(\mathbf{r}) \; \rho_{if}(\mathbf{r}) \; \Psi_{NLM}(\mathbf{r}) \right|^2 \right\rangle \frac{d\Omega_{q_f}}{4\pi}. \tag{2.17}$$

An important quantity is the capture rate per one stopped kaon R_{if} which is simply the ratio between the capture rate of one process Γ_{if} and the sum of rates to all possible final states $\Gamma = \sum_f \Gamma_{if}$ (= total capture rate):

$$R_{if} = \frac{\Gamma_{if}}{\Gamma}. \tag{2.18}$$

The summation over all hypernuclear states can be obtained by applying the relation of closure

$$\frac{1}{2J_i + 1} \sum_{M_i} \sum_f \rho^*_{if}(\mathbf{r}') \rho_{if}(\mathbf{r}) = \rho_N \delta(\mathbf{r}' - \mathbf{r}), \tag{2.19}$$

where ρ_N is the density of nucleons of the type N normalized to their number. Consequently,

$$\Gamma = \gamma(K^- N \to all) \int \mathrm{d}^3\mathbf{r} \; \rho_N(r) \, \rho_{K^-}(r) \, \rho_\pi(r), \tag{2.20}$$

where

$$\rho_{K^-}(r) = \frac{1}{2L+1} \sum_M |\Psi_{NLM}(\mathbf{r})|^2 \;\; , \quad \rho_\pi(r) = \int |\chi_{q_f}(\mathbf{r})|^2 \frac{\mathrm{d}\Omega_{q_f}}{4\pi}.$$

Gal and Klieb [21] neglected the influence of the distortion of outgoing pion and replaced its wave function in formula (2.20) by a simple plane wave ($\rho_\pi = 1$). If we introduce the effective nucleon density available to the capture process $\widetilde{\rho}_N$, the approximation can be written as

$$\widetilde{\rho}_N = \int \mathrm{d}^3\mathbf{r} \; \rho_N(r) \, \rho_{K^-}(r) \, \rho_\pi(r) \approx \int \mathrm{d}^3\mathbf{r} \; \rho_N(r) \, \rho_{K^-}(r). \tag{2.21}$$

As we will demonstrate in Chapter 4, this simplification is not fully justified. The quantity $\widetilde{\rho}_N$ provides the normalization of the overlap of the pertinent wave functions (2.14).

The final formula for the capture rate per one stopped kaon can be written as a product of three terms

$$R_{if} = \frac{q_f \omega_f}{\overline{q}_f \overline{\omega}_f} \cdot R(K^- N \to \pi Y) \cdot R_{if}/Y. \tag{2.22}$$

The first term in (2.22) is the kinematic factor. This factor appears due to the fact that the process takes place in the nuclear medium and the momentum of a nucleon is not equal to the momentum of the whole nucleus.

The second term in (2.22) is the branching ratio for the elementary process

$$R(K^- N \to \pi Y) = \frac{\overline{\gamma}(K^- N \to \pi Y)\widetilde{\rho}_N}{\overline{\gamma}(K^- p \to \text{all})\widetilde{\rho}_p + \overline{\gamma}(K^- n \to \text{all})\widetilde{\rho}_n}. \tag{2.23}$$

The last term, which we call the capture rate per hyperon, is

$$R_{if}/Y = \frac{\int \left\langle \left| \int \mathrm{d}^3 r \; \chi_{q_f}^{(-)^*}(\mathbf{r}) \; \rho_{if}(\mathbf{r}) \; \Psi_{NLM}(\mathbf{r}) \right|^2 \right\rangle \frac{d\Omega_{q_f}}{4\pi}}{\widetilde{\rho}_N}. \tag{2.24}$$

We focus on the capture rate per hyperon (2.24) and the elementary branching ratio (2.23) in the following two subsections.

2.2.1 Capture rate per hyperon

Now, we try to simplify the capture rate per hyperon (2.24) analytically. It is useful to work in spherical coordinates and use the partial wave expansion. The K^- wave function is

$$\Psi_{NLM}(\mathbf{r}) = R_{NL}(r) \; Y_{LM}(\Omega_r). \tag{2.25}$$

The outgoing pion wave function can be written in the partial wave expansion as

$$\chi_{q_f}^{(-)^*} = \sum_l i^{-l} \, (2l+1) \widetilde{j}_l(r) P_l(\hat{\mathbf{q}}.\hat{\mathbf{r}}). \tag{2.26}$$

The nucleon (and hyperon) wave function can be written as

$$\psi_{nljm}(\mathbf{r}) = \frac{u_{nlj}(r)}{r} \left[Y_l(\hat{\mathbf{r}}) \otimes \chi_{1/2} \right]^j_m . \tag{2.27}$$

The effective nuclear density standing in the denominator of (2.24) becomes

$$\widetilde{\rho}_N = \int \mathrm{d}r \; \rho_N(r) \, |R_{NL}(r)|^2 \sum_l (2l+1) |\widetilde{j}_l(r)|^2. \tag{2.28}$$

The integral in the numerator of (2.24), let us denote it **I**, is more complicated. Its complete evaluation is detailed in Appendix B. Here, we present only the most important partial results and further assumptions and approximations. The integral can be directly transferred to the form

$$\begin{aligned} \mathbf{I} \;=\; & \frac{1}{2J_i+1} \sum_{kl} (l0\,k0|L0)^2 \left| \sum_{n_Y j_Y l_Y} \sum_{n_N j_N l_N} I^l_{\gamma_Y \gamma_N} (-1)^{(j_N + l_N + 1/2)} \right. \\ & \sqrt{(2j_Y+1)(2j_N+1)(2l_N+1)} (l_N 0 k 0 | l_Y 0) \begin{Bmatrix} j_N & j_Y & k \\ l_Y & l_N & 1/2 \end{Bmatrix} \\ & \left. < H \| (a^+_{n_Y l_Y j_Y} \otimes \widetilde{a}_{n_N l_N j_N})^k \| A > \right|^2 , \end{aligned} \tag{2.29}$$

where $I^l_{\gamma_Y \gamma_N}$ is the integral over radius r

$$I^l_{\gamma_Y \gamma_N} = \int_0^\infty \mathrm{d}r \; u^*_{n_Y j_Y l_Y}(r) \, u_{n_N j_N l_N}(r) \, \tilde{j}_l(r) \, R_{NL}(r). \tag{2.30}$$

We assume that the capture occurs from one particular nucleon shell $n_N l_N$ to one particular hyperon shell $n_Y l_Y$. Now, we can sum over all possible final states. After further manipulations (see Appendix B), we obtain

$$\mathbf{I}_{n_N l_N \to n_Y l_Y} = \sum_{k, j_Y, j_N} (2k+1)(2l_N+1)(2j_Y+1) \begin{Bmatrix} j_N & j_Y & k \\ l_Y & l_N & 1/2 \end{Bmatrix}^2 N^{(k)}_{\gamma_Y \gamma_N} N(j_N), \tag{2.31}$$

where

$$N^{(k)}_{\gamma_Y \gamma_N} = \sum_l (L0\,k0|l0)^2 |I^l_{\gamma_Y \gamma_N}|^2,$$

and $N(j_N)$ is the number of nucleons in the shell j_N.

We assume that the integral $I^l_{\gamma_Y\gamma_N}$ depends only weakly on the j_Y or j_N quantum numbers. We can then neglect this dependence and perform the last summation over j_Y considering the capture in the particular shell j_N.

The final result for the capture rate per one hyperon then becomes

$$R_{n_N l_N \to n_Y l_Y}/Y = \frac{N(j_N)\sum_k (2k+1)(l_N 0 k 0|l_Y 0) N^{(k)}_{\gamma_Y\gamma_N}}{\int \mathrm{d}r\ \rho_N(r)\,|R_{NL}(r)|^2 \sum\limits_l (2l+1)|\widetilde{j}_l(r)|^2}\,. \tag{2.32}$$

The letter k is not a mere summation index but also represents the multipolarity of the process. Its value equals to the value of the transferred orbital momentum. The value of k is usually used for classification of nuclear processes.

2.2.2 Elementary branching ratio

Here, we focus on the elementary branching ratio (2.23), which is the second term in the formula for the capture rate per one stopped kaon (2.22). The branching ratios (2.23) for the elementary processes $n(K^-,\pi^-)\Lambda$ and $p(K^-,\pi^0)\Lambda$ were obtained using the chirally motivated effective separable potentials (presented in section 2.1).

The low energy constants (parameters) of the model are taken from the Cieply and Smejkal [26] (to be specific from the parameter set corresponding to $\sigma_{\pi N} = 40$ MeV). They were fitted to a wide range of experimental data on K^-p reactions.

When the required branching ratios $R(K^-N \to \pi\Lambda)$ are calculated in the nuclear medium the model gives a decreasing function of the nucleon density, as demonstrated in figure 2.

We assume that the reaction takes place at a proton (or neutron) density $\rho = \rho_0/2$ ($\rho_0 = 0.17$ fm^{-3}). Although the central density in different nuclei varies (from 0.14 up to 0.22 fm^{-3}), the branching ratios do not change much in this region. Therefore, we can neglect this dependence. For future purposes, we denote the branching ratios obtained

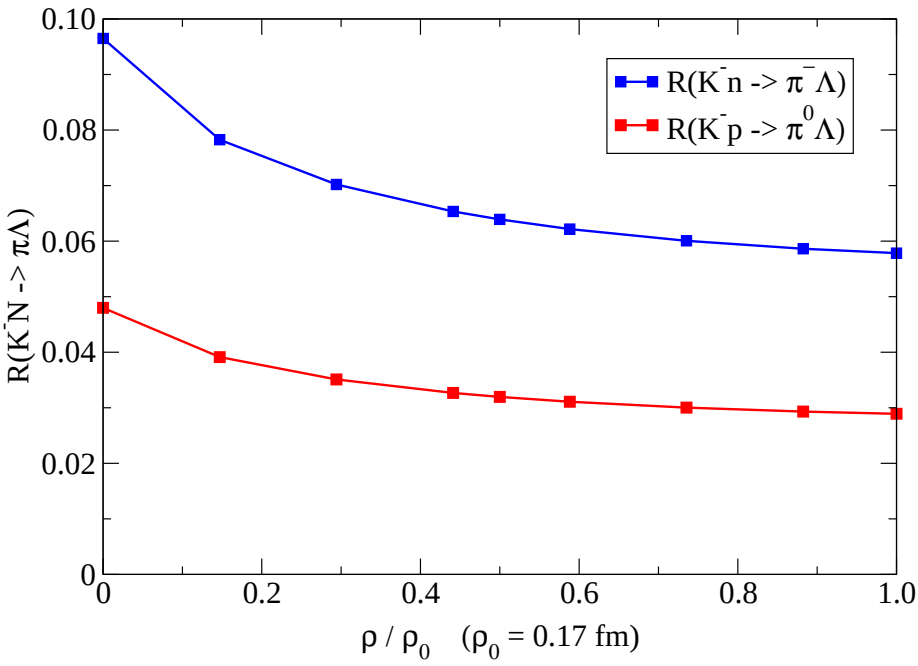

Figure 2: The dependance of branching ratios on the nucleon density.

at the nucleon density $\rho = \rho_0/2$ by I and the branching ratios obtained when the effect of nuclear medium is neglected by II.

The use of a microscopic model for the elementary branching ratios is one of the novelties of our work. The previous authors used branching ratios derived from experiment [21, 31]. However, the values were not measured directly, but were extrapolated from the measurements done on carbon and freon. We find this approach quite ambiguous and prone to systematic errors, due to not so well known factors. Therefore, we feel that the elementary branching ratios obtained this way do not describe the elementary process accurately. We denote them by III for comparison with branching ratios obtained by our microscopic model.

The pertinent elementary branching ratios are shown in Table 1.

Table 1: Elementary branching ratios (in units 10^{-2}).

	I	*II*	*III*	
branching ratio	$\rho = \rho_0/2$	$\rho = 0$	^{12}C	^{16}O
$R(K^- n \to \pi^- \Lambda)$	6.39	9.65	8.7	7.7
$R(K^- p \to \pi^0 \Lambda)$	3.20	4.80	4.4	3.9

Chapter 3

Input wave functions

To perform the numerical calculation of two integrals, $I^l_{\gamma_Y \gamma_N}$ (2.30) and $\widetilde{\rho}_N$ (2.28), which are essential to obtain the capture rate of the process, we need the wave functions of the kaon, nucleon, hyperon and the outgoing pion. The wave functions of bound states (nucleon, hyperon, kaon) were obtained numerically using the Numerov method. The code for computing the wave functions of bound states was written by the author. We use a standard computer code written for pion scattering [32] to get the pion wave functions.

3.1 Nucleon and hyperon wave functions

The wave functions of nucleons and hyperons were computed numerically as bound states in a Wood-Saxon potential

$$V(r) = -\frac{V_0}{1 + \exp\left(r - R\right)/a} \ , \ \ R = r_0\, A^{1/3}\,. \tag{3.1}$$

The geometry was fixed by setting $a = 0.6$ fm and $r_0 = 1.25$ fm. The potential depth V_0 was adjusted separately for each baryon state so that the corresponding binding energy was reproduced. The values of the binding energies are shown in Table 2 [2, 21].

Table 2: Baryon binding energies in MeV.

nucleon orbit	p	n	Λ
$A = 12$			
$1s_{1/2}$	34.1	37.3	10.8
$1p_{3/2}$	16.0	18.9	0.3
$A = 16$			
$1s_{1/2}$	32.0	35.3	12.4
$1p_{3/2}$	18.3	21.8	3.1
$1p_{1/2}$	12.1	15.7	1.5

We tested the sensitivity of our results to the baryon wave functions. For this purpose we calculated the capture rate for the production of ${}^{12}_{\Lambda}$C in both $1S_\Lambda$ and $1P_\Lambda$. To test the sensitivity to the geometry of the potential, we used the number $A = 11$ instead of $A = 12$ in the expression for the Wood-Saxon potential. The difference appeared to be less than 10%. To test the sensitivity to the depth of the potential, we calculated baryon wave functions for binding energy about 10% higher and smaller. The difference appeared to be less than 5%. Since the sensitivity to the baryon wave functions is quite small and its testing is not the purpose of this work, we will not focus on it any more.

3.2 K^--atomic wave function

We use the Klein-Gordon equation with a potential that consists of two parts, the Coulomb potential with finite size effects and the optical potential describing strong interaction, which was taken from [33]:

$$V^K_{opt}(r) = -\frac{4\pi}{2\mu}\left(1 + \frac{\mu}{M_N}\right)\left[b + B\left(\frac{\rho(r)}{\rho(0)}\right)^\nu\right]\rho(r). \tag{3.2}$$

Here μ is the kaon reduced mass, M_N is the nucleon mass and $\rho(r)$ is the nuclear density normalized to the number of nucleons A. We use three different parameter sets for the kaon-nucleus optical potential, which are specified in Table 3. Moreover, we consider also a pure Coulomb potential ([coul]) for comparison. We denote the different optical potentials and corresponding wave functions by abbreviations in square brackets.

Table 3: Parameters of the kaonic optical potential.

set	b [fm]	B [fm]	ν
[eff]	$0.63 + 0.89\mathrm{i}$	0	0
[DD]	$-0.15 + 0.62\mathrm{i}$	$1.65 - 0.06\mathrm{i}$	0.23
[chir]	$0.69 + 2.02\mathrm{i}$	0	0

The meson-nuclear optical potential is usually expressed as the scattering length multiplied by the nuclear density. Thus, the parameter b for potential [chir] is the average of the K^-n and K^-p scattering lengths in the nuclear medium computed using the chiral model presented in sections 2.1 and 2.2.2. The values of the parameter sets [eff] and [DD] were fitted to reproduce a large set of kaonic atom data by Friedman et al [33]. In order to be consistent, we use the same parametrization of the nuclear density as the authors of ref. [33]. They described the nuclear density using a modified harmonic oscillator model [34]:

$$\rho(r) = \rho_0 \left(1 + \alpha \frac{r^2}{R^2}\right) e^{-\frac{r^2}{R^2}}.$$

The parameters α and R for the relevant nuclei are listed in Table 4.

For $B = 0$, the potential reduces to the standard "effective" ([eff]) parametrization of the optical potential. The solution [DD] exhibits another explicit density dependence, because of nonzero parameters B and ν. If we consider the central nuclear density $\rho_0 = 0.17$ fm^{-3}, the depth of the potential (its real part) equals to 83 MeV for potential [eff], 193 MeV for [DD] and 91 MeV for [chir].

Table 4: Parameters of the nuclear density.

nuclei	α	R [fm]
^{12}C	2.234	1.516
^{16}O	3.027	1.629

The real and imaginary parts of wave functions for the $2P$ K^--atomic states in ^{12}C are shown in figures 3 and 4 to illustrate the difference between various parameter sets.

3.3 Pion wave function

The pionic optical potential is taken to be of the standard form [35], usually used in the analysis of pionic atoms and pion-nuclear scattering:

$$\begin{aligned} -\frac{2\mu_\pi}{4\pi}V^\pi_{opt} &= \left(1+\frac{m_\pi}{M}\right)b_0\rho(r)+\left(1+\frac{m_\pi}{2M}\right)B_0\rho^2(r)-\nabla\frac{\alpha(r)}{1+\frac{4\pi}{3}\xi\alpha(r)}\nabla \quad (3.3)\\ \alpha(r) &= \left(1+\frac{m_\pi}{M}\right)^{-1}c_0\rho(r)+\left(1+\frac{m_\pi}{2M}\right)^{-1}C_0\rho^2(r). \end{aligned}$$

We perform our calculations with a free pion (plane wave) and with two different parameter sets for the pion-nuclear optical potential [36, 37]. We denote the different parameter sets and corresponding wave functions by letters in round brackets. The parameters are in Table 5.

Table 5: Parameters of the pionic optical potential.

set	b_0 $[m_\pi^{-1}]$	B_0 $[m_\pi^{-4}]$	c_0 $[m_\pi^{-3}]$	C_0 $[m_\pi^{-6}]$	ξ
(b)	$0.268+0\mathrm{i}$	0	$0.036+0.206\mathrm{i}$	$0-0.203\mathrm{i}$	1.4
(c)	$0.010+0.437\mathrm{i}$	0	$0.047+0.222\mathrm{i}$	0	0

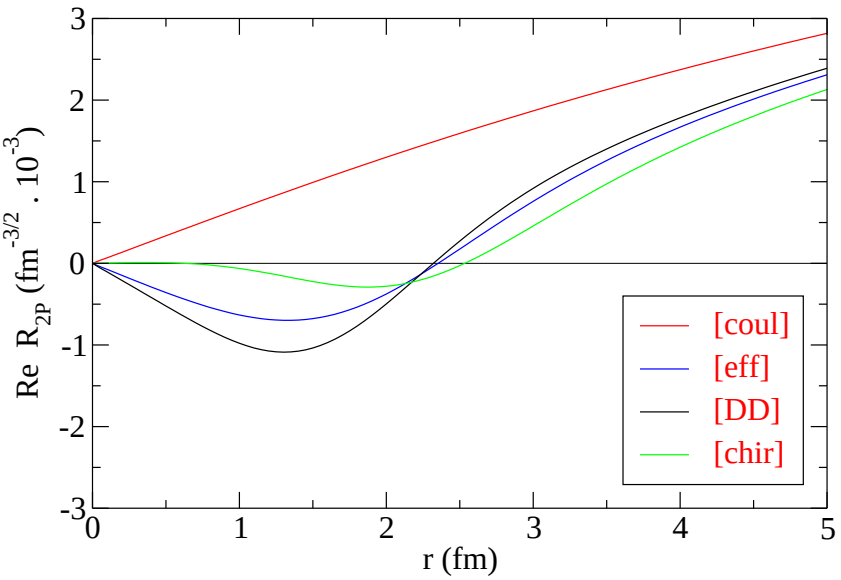

Figure 3: Real part of the K^- wave function in the $2P$ state in ^{12}C.

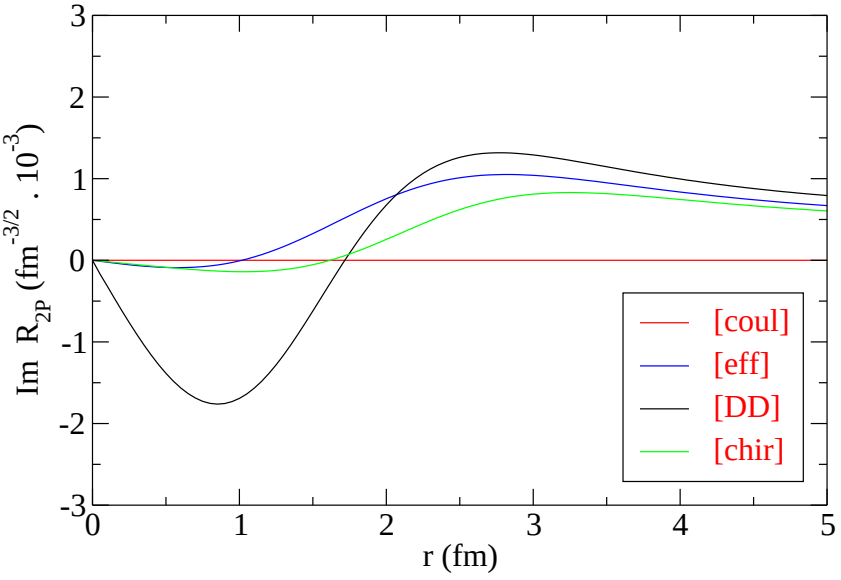

Figure 4: Imaginary part of K^- wave function in the $2P$ state in ^{12}C.

Chapter 4

Results and discussion

In this chapter, we present the results of numerical calculations of the capture rate per stopped kaon and discuss their sensitivity to different input wave functions (i.e. different kaon-nucleus, resp. pion-nucleus optical potentials), to different branching ratios for elementary process (taken from microscopic model or derived from experiments), to the neglect of the pion distortion in the effective nucleon density available to the process, and to other possible effects.

The capture rate per stopped kaon R_{fi}, the quantity we are interested in, is given by formula (2.22). It consists of three terms, the kinematic factor, the branching ratio for the elementary process and the capture rate per hyperon.

The detailed description of input branching ratios and wave functions is in the previous chapters. We take the value 1.4 [21] for the kinematic factor $q_f\omega_f/\overline{q}_f\overline{\omega}_f$. We consider three different values of branching ratios for the elementary processes. The first one is derived within the microscopic model and includes the effect of the nuclear medium (I), the second one is derived from the microscopic model in the vacuum (II) and the third one is derived from the experiment (III).

The capture rate per hyperon (2.24) contains two integrals of wave functions, one in the numerator (2.30) and one in the denominator (2.28), which have to be computed

numerically. We also compare the results using the effective nuclear density $\widetilde{\rho}_N$ with and without the effect of pion distortion (2.21, 2.28).

We calculated the processes of the hypernuclear production from nuclei ^{12}C and ^{16}O and considered only the formation of Λ-hypernuclei ($^{12}_{\Lambda}$C, $^{12}_{\Lambda}$B, $^{16}_{\Lambda}$O, $^{16}_{\Lambda}$N). We took into account two baryon transitions $1P_N \to 1S_\Lambda$ and $1P_N \to 1P_\Lambda$, where the hyperon is created in the $1S$ and $1P$ state, respectively. Both processes take place on a nucleon in the $1P$ state, which is the valence orbit, and we believe that the reaction takes place just on the valence nucleon. There is only one possible value of the multipolarity k of the process in the first case, $k = 1$, and there are two possible values of k in the second case, $k = 0$ and $k = 2$.

We assume two K^- atomic orbits, $2P$ and $3D$, and perform the calculations separately for each orbit. Finally, we average over the states due to the estimated population of the orbits [38]. The relative population of orbits is in Table 6.

Table 6: Relative population of K^--atomic orbits.

	^{12}C	^{16}O
2P	0.23	0.18
3D	0.77	0.82

Before we proceed to comparison of our results with experiment and previous theoretical works, we show the sensitivity of the presented model to some effects.

First, we discuss the sensitivity to the choice of branching ratios for the elementary process. In figure 5, we present the capture rate for the production of $^{12}_{\Lambda}$C in the $1S_\Lambda$ state for the K^--nucleus potential [eff] and pion-nucleus potential (c). We recall that the branching ratios I and II come from our microscopic model and III are derived from experiment.

We can see that all the calculated values are quite close to each other but significantly

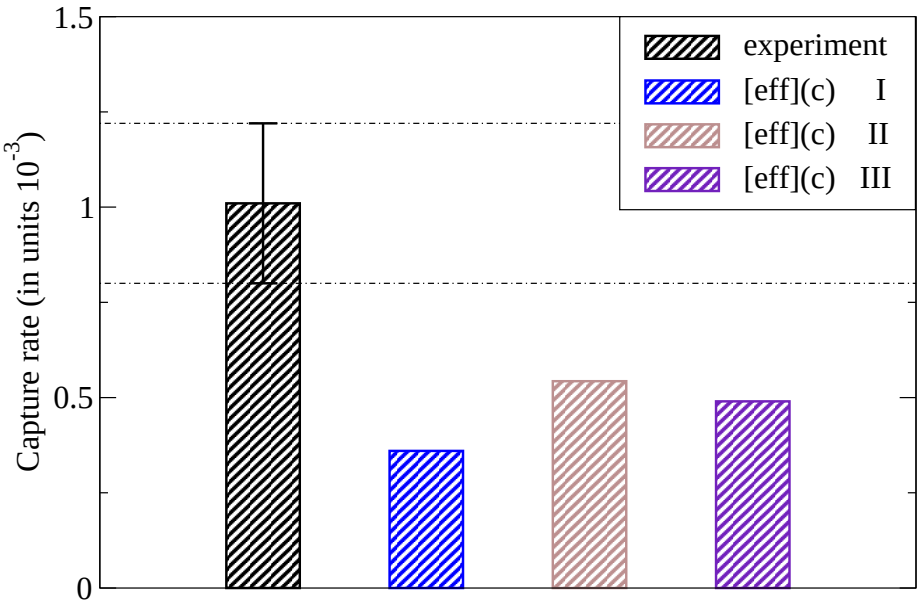

Figure 5: The sensitivity of the capture rate to elementary branching ratios.

below the experimental data. The value where we use the branching ratios from the microscopic model without considering the effect of the nuclear medium (II) is highest, and the value where we use the branching ratio from microscopic model and considered the effect of nuclear medium (I) is smallest. The value where we used branching ratio derived from experiment (III) lies between. We prefer the theoretical approach (discussed in Chapter 2), and we believe that the most accurate description is provided by the branching ratio I. Because the difference between the results corresponding to various elementary branching ratios (50% at most) is smaller than the difference between the calculated capture rates and the experimental value (100% at least), we expect that there are other effects (kaon-nucleus potential, pion-nucleus potential, effective nuclear density), which influence the numerical results more. Consequently, all further results correspond to the elementary branching ratios I.

Next, we discuss the sensitivity of the results to the effective nucleon density (2.21, 2.28), which stands in the denominator of the capture rate per hyperon (2.32). We consider $\{C\}$ or neglect $\{N\}$ the effect of pion distortion. In figure 6, we demonstrate the effect for the [DD] K^--nucleus potential for both (b) and (c) pion-nucleus potentials. The calculated capture rate is the one for the production of ${}^{12}_{\Lambda}$B in the $1S_\Lambda$ state

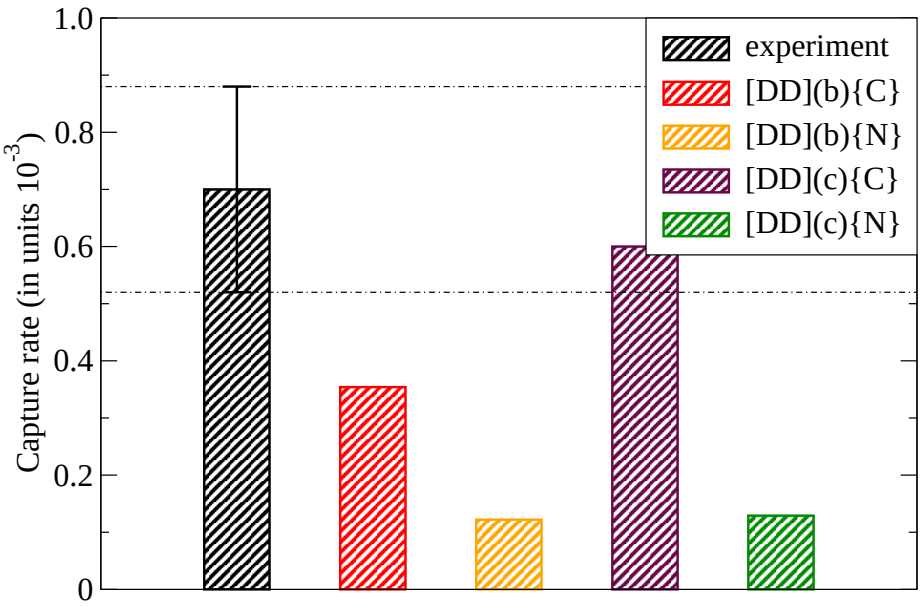

Figure 6: The sensitivity of the capture rate to the effective nucleon density.

The proper treatment of the pion distortion in the effective nucleon density leads to a substantial effect on the capture rate. The results for the pion-nucleus potentials (b) and (c) are about three times and even five times higher, respectively, if we consider the pion distortion in the expression for the effective nucleon density (2.21). As a result, the computed values for the capture rate get much closer to the experimental value. The authors of previous papers [18, 21, 22] neglected this effect, but our results indicate that this assumption is not justified. Thus, all the following results are calculated including

the pion distortion in the effective nucleon density.

Next, we demonstrate the sensitivity to the K^- wave functions. In the figure 7, we show the capture rate for the creation of ${}^{12}_{\Lambda}\mathrm{C}$ with the hyperon in $1P_\Lambda$ state (figures for other processes look similar). The pion wave function (b) is used in this figure.

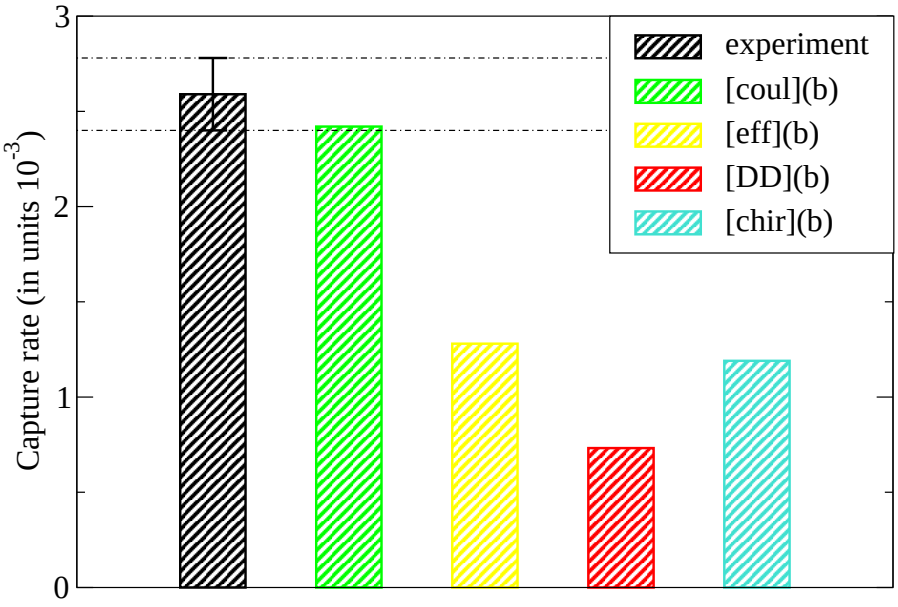

Figure 7: The sensitivity of the capture rate to the K^- wave function.

We can see that the capture rate is highest, and thus closest to the experimental value, for the kaon-nucleus potential [coul], where the strong interaction is completely neglected. The values for potentials [eff] and [chir] are about one half of the value for [coul] and the value for [DD] K^--nucleus potential is the smallest. Since the [DD] optical potential is about twice as deep as potentials [eff] and [chir], which are of the comparable depth, and the [coul] potential contains no strong interaction part at all, we can conclude that the capture rate is a decreasing function of the kaon-nucleus potential depth. The [coul] potential does not describe the K^--nucleus interaction properly, therefore the fact

that the result for the [coul] potential is so close to the experimental value indicates that there are other effects we did not consider in our calculations. If we focus on the other K^--nucleus potentials, where the agreement with experiment is not so satisfactory. Our best result is about 50% smaller than the experimental value.

Figure 8 shows the dependence of the capture rate on a choice of the pion-nucleus potential for the creation of ${}^{16}_{\Lambda}\mathrm{O}$ in the $1P_\Lambda$ state. The K^- wave function corresponding to the potential [eff] is considered in this figure.

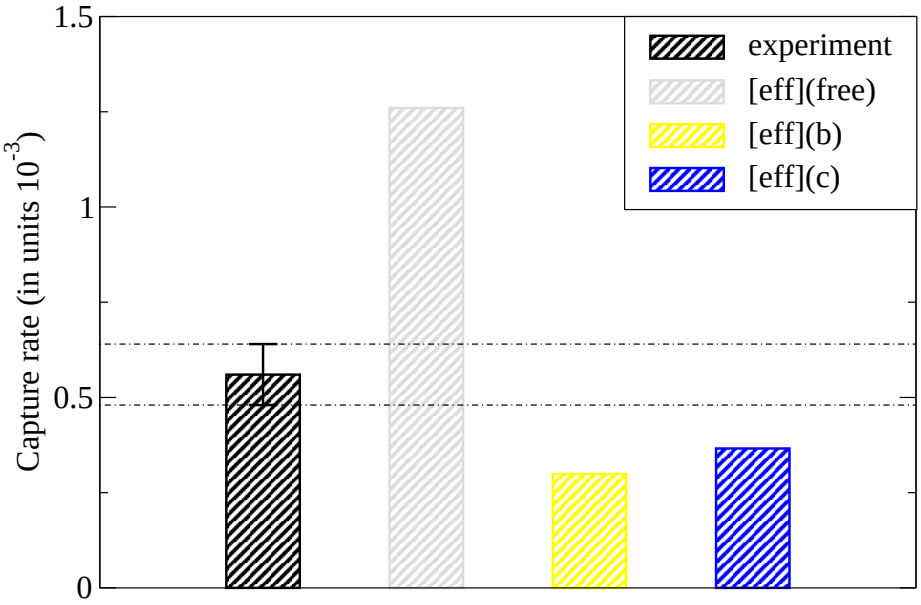

Figure 8: The sensitivity of the capture rate to the pion wave function.

We see that pion distortion plays an important role. The difference between the results of calculations with and without pion distortion is significant. On the other hand, the difference between the results for two different (but non-zero) pion-nucleus optical potentials is much smaller. The result for the potential (c) is a little higher than the result for the potential (b). The experimental value lies between values computed

with the free and with the distorted pion.

The results of all processes we calculated are summarized in Tables 7-10. The experimental data for the production of ${}^{12}_{\Lambda}$C [8], ${}^{12}_{\Lambda}$B [20], and ${}^{16}_{\Lambda}$O [19] are shown for comparison. The measurement of ${}^{16}_{\Lambda}$N has not been performed yet, so our results for this process are pure predictions.

Before we make the comparison of our results with experimental data and previous theoretical predictions, we determine the best combination of potentials involved in our calculations. To obtain the combination of potentials, which is in the best agreement with experimental data, we calculate the standard weighted least square test (χ^2 test)

$$\chi^2 = \sum_i \frac{(X_i - X_i^{exp})^2}{\sigma_i^2}. \tag{4.1}$$

We take into account six processes, for which we have direct experimental data (the production of ${}^{12}_{\Lambda}$C in the $1S_\Lambda$ and $1P_\Lambda$ state, the production of ${}^{12}_{\Lambda}$B in the $1S_\Lambda$ and $1P_\Lambda$ state, the production of ${}^{16}_{\Lambda}$O in the $1S_\Lambda$ and $1P_\Lambda$ state) and four ratios between capture rates (the ratio between the $1P$ and $1S$ production for ${}^{12}_{\Lambda}$C, the ratio between the $1P_\Lambda$ and $1S_\Lambda$ production for ${}^{16}_{\Lambda}$O, the ratio between the production of ${}^{12}_{\Lambda}$C and ${}^{16}_{\Lambda}$O in the $1S_\Lambda$ state and the ratio between production of ${}^{12}_{\Lambda}$C and ${}^{16}_{\Lambda}$O in the $1P_\Lambda$ state). The results of this procedure are summarized in Table 11.

The best agreement with the experiment is clearly for the combination of the [coul] potential for the K^--nuclear interaction and the (b) potential for pion-nuclear interaction. If we consider only the combinations with the strong interaction included, then the combination of potentials [eff] and (c) is the best one. Below, we compare the results for this combination of potentials with experiment and previous theoretical calculations. Table 11 clearly demonstrates that the kaon-nucleus potentials [DD] and [chir] yield much worse agreement with the experimental data than the K^--nucleus potential [eff].

Table 7: Total capture rates for the production of ${}^{12}_{\Lambda}$C (in units 10^{-3}).

transition	[coul] (free)	[coul] (b)	[coul] (c)	[eff] (free)	[eff] (b)	[eff] (c)	[DD] (free)	[DD] (b)	[DD] (c)	[chir] (free)	[chir] (b)	[chir] (c)	exp
$1P_\Lambda(3/2) \to 1S_\Lambda(1/2)$	1.43	0.79	0.79	1.42	0.34	0.36	1.52	0.22	0.15	0.92	0.20	0.23	1.01 ± 0.21
$1P_\Lambda(3/2) \to 1P_\Lambda(3/2)$	3.69	2.42	3.02	3.30	1.82	1.71	2.21	0.73	1.11	2.96	1.19	1.52	2.59 ± 0.19

Table 8: Total capture rates for the production of ${}^{12}_{\Lambda}$B (in units 10^{-3}).

transition	[coul] (free)	[coul] (b)	[coul] (c)	[eff] (free)	[eff] (b)	[eff] (c)	[DD] (free)	[DD] (b)	[DD] (c)	[chir] (free)	[chir] (b)	[chir] (c)	exp
$1P_\Lambda(3/2) \to 1S_\Lambda(1/2)$	0.69	0.38	0.39	0.69	0.16	0.18	0.75	0.10	0.08	0.46	0.10	0.12	0.56 ± 0.16
$1P_\Lambda(3/2) \to 1P_\Lambda(3/2)$	1.81	1.29	1.57	1.65	0.62	0.90	0.96	0.35	0.60	1.51	0.67	0.81	0.70 ± 0.18

Table 9: Total capture rates for the production of ${}^{16}_{\Lambda}$O (in units 10^{-3}).

transition	[coul] (free)	[coul] (b)	[coul] (c)	[eff] (free)	[eff] (b)	[eff] (c)	[DD] (free)	[DD] (b)	[DD] (c)	[chir] (free)	[chir] (b)	[chir] (c)	exp
$1P_\Lambda(1/2) \to 1S_\Lambda(1/2)$	0.35	0.15	0.15	0.37	0.05	0.05	0.42	0.03	0.02	0.20	0.02	0.03	0.13 ± 0.04
$1P_\Lambda(1/2) \to 1P_\Lambda(3/2)$	1.41	0.71	0.80	1.26	0.30	0.37	0.89	0.19	0.24	0.89	0.23	0.28	0.56 ± 0.08

Table 10: Total capture rates for the production of ${}^{16}_{\Lambda}$N (in units 10^{-3}).

transition	[coul] (free)	[coul] (b)	[coul] (c)	[eff] (free)	[eff] (b)	[eff] (c)	[DD] (free)	[DD] (b)	[DD] (c)	[chir] (free)	[chir] (b)	[chir] (c)
$1P_\Lambda(1/2) \to 1S_\Lambda(1/2)$	0.17	0.07	0.07	0.18	0.03	0.03	0.21	0.02	0.01	0.09	0.01	0.01
$1P_\Lambda(1/2) \to 1P_\Lambda(3/2)$	0.65	0.37	0.44	0.61	0.15	0.18	0.43	0.09	0.12	0.46	0.13	0.16

Table 11: The χ^2 test for all sets of potentials.

potentials	χ^2	potentials	χ^2	potentials	χ^2	potentials	χ^2
[coul](free)	229.0	[eff](free)	168.0	[DD](free)	99.6	[chir](free)	50.1
[coul](b)	21.7	[eff](b)	84.6	[DD](b)	154.5	[chir](b)	167.6
[coul](c)	47.2	[eff](c)	65.9	[DD](c)	212.3	[chir](c)	138.8

The comparison of our calculations with experimental data [8, 19, 20] and previous theoretical works is shown in figures 9-13. We present both the production capture rates and the ratios between the capture rates. The theoretical predictions of Gal and Klieb [21] are denoted by GL. The theoretical predictions of Matsuyama and Yazaki [22] are denoted by MY, and the predictions of Cieply et al [18] are denoted by CFGM.

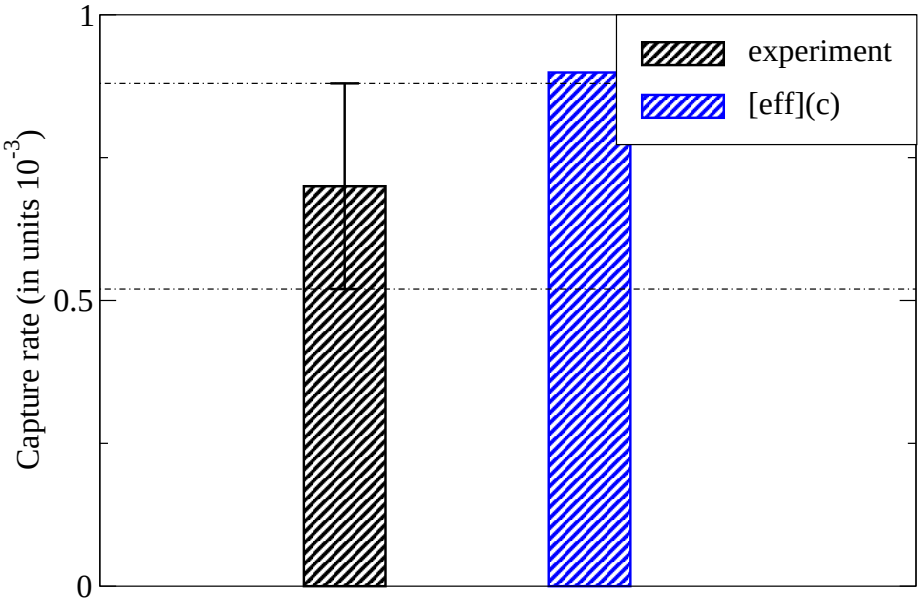

Figure 9: The production of ${}^{12}_{\Lambda}$B in the $1P_\Lambda$ state.

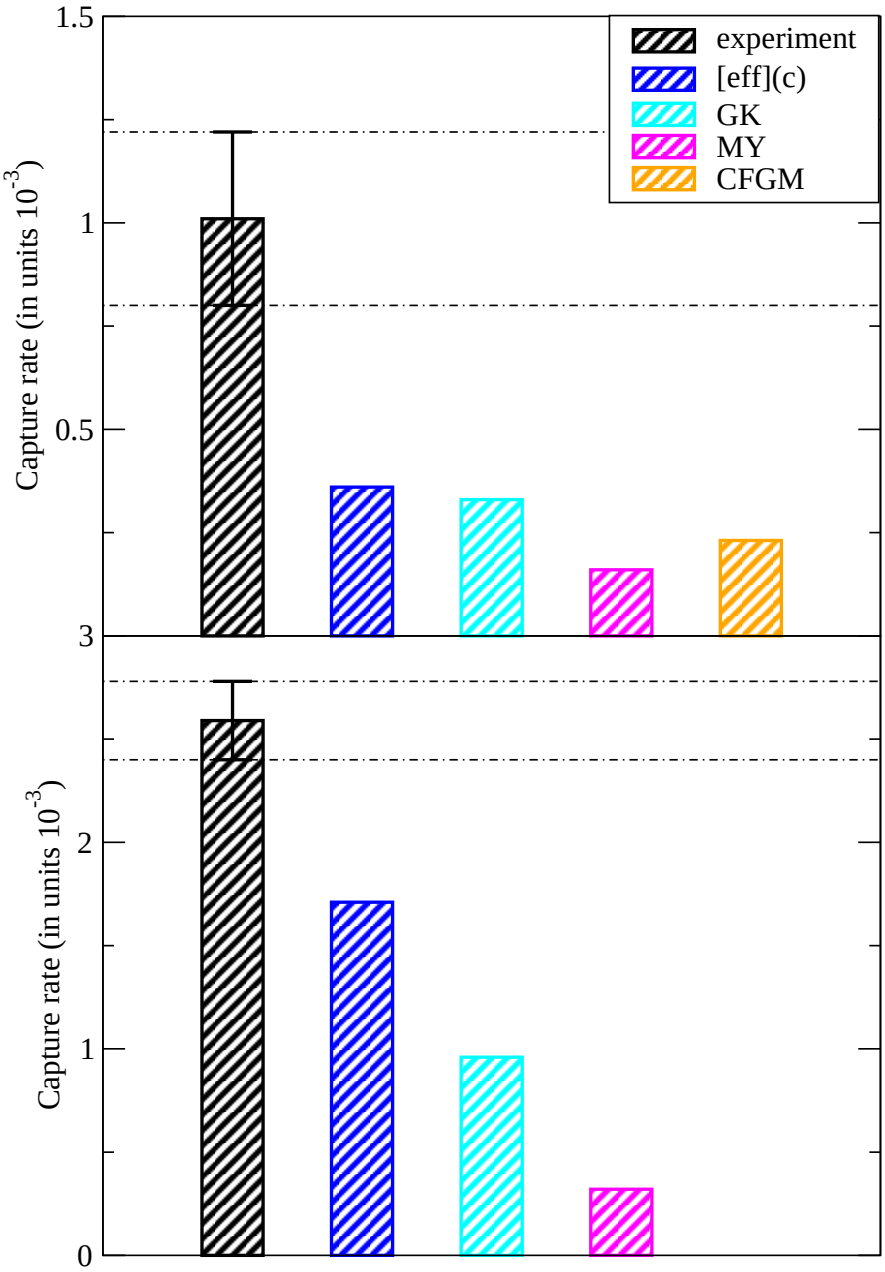

Figure 10: The production of ${}^{12}_{\Lambda}$C in the $1S_\Lambda$ (top) state and in the $1P_\Lambda$ state (bottom).

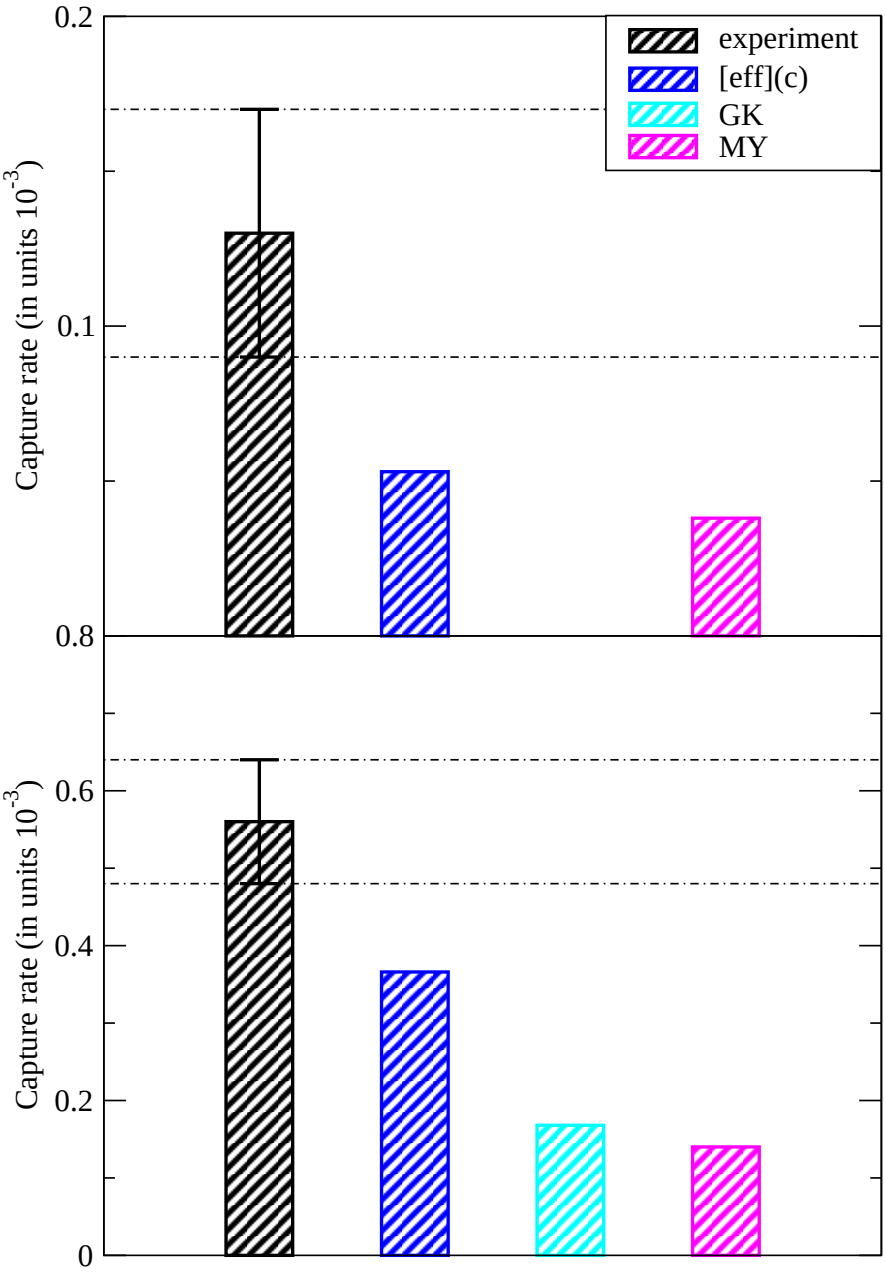

Figure 11: The production of ${}^{16}_{\Lambda}$O in the $1S_\Lambda$ (top) state and in the $1P_\Lambda$ state (bottom).

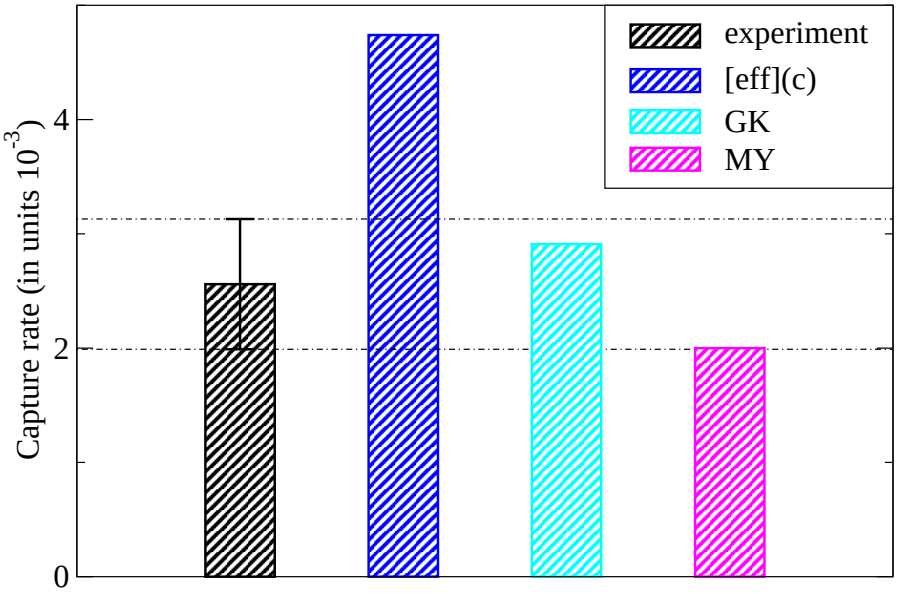

Figure 12: The ratio between the capture rates to $1P_\Lambda$ and $1S_\Lambda$ states for the production of ${}^{12}_{\Lambda}\mathrm{C}$.

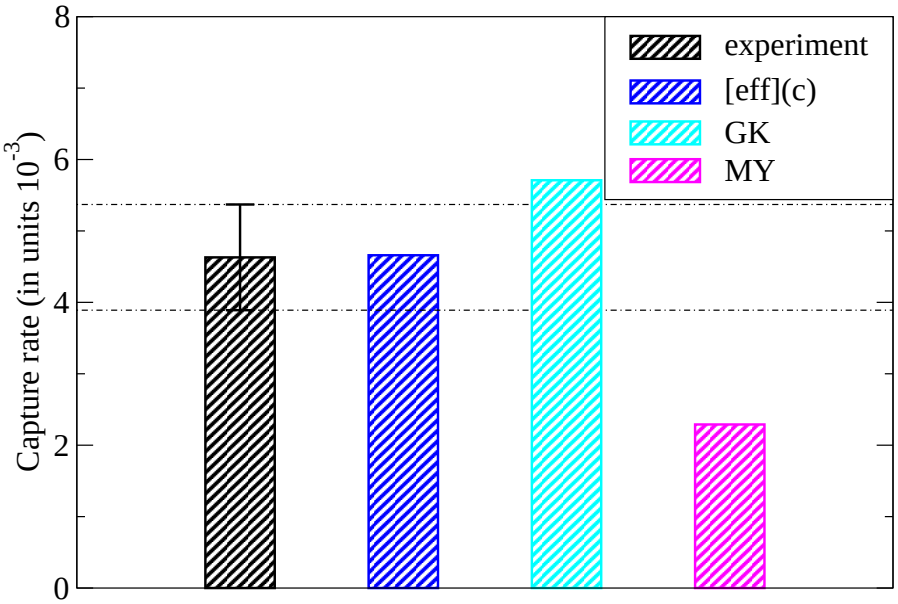

Figure 13: The ratio between the capture rates for the production of ${}^{12}_{\Lambda}\mathrm{C}$ and ${}^{16}_{\Lambda}\mathrm{O}$ to the $1P_\Lambda$ state.

We see that our results are in better agreement with experimental data than results of previous authors. To be more quantitative we calculate the χ^2 test (4.1) for the available results. In the test, we include only those processes that are calculated by the authors of the previous papers. The comparison of our results with previous calculations is in the Table 12.

Table 12: The χ^2 test.

	GK	MY	CFGM
χ^2 previous	110.6	204.4	13.8
χ^2 present	52.0	55.8	9.6

Although our results are better than the results of other authors, the agreement with experimental data is still unsatisfactory. Therefore, we have to look for some other effects that could explain the discrepancy:

First, the wide range of the calculated capture rates for different pion wave functions indicates huge sensitivity to the pion optical potential. The optical potentials considered in this work were developed for interaction of pions with ordinary nuclei. The interaction of the pion with hypernuclei could be different, but specific models of the pion-hypernucleus and pion-hyperon interaction as well as experimental data for such processes are not available yet. Including the effects of the pion-hyperon interaction could modify the wave function of the outgoing pion. In addition, the momentum of outgoing pion in the $K^-_{\rm stopped}$ reactions is about 260-280 MeV. In this energy region, the $\Delta(1232)$ resonance might play an important role. However, its effect has not been considered at all.

Second, the structure of a hypernucleus was not considered at all. The hyperon wave function in a hypernucleus was computed using the Wood-Saxon potential with the same range parameters as those that were used for the nucleon wave function in a

standard nucleus, although the structure of a hypernucleus could be different.

Third, the K^--nuclear wave function of deeply bound state could be used, instead of K^--atomic wave functions. Using atomic wave functions (kaon) on one hand and nuclear wave function (nucleon, hyperon) on the other may look illogically. Since we have no information about experimental evidence of transition from atomic to nuclear states, we do not take K^--nuclear states into account.

Finally, the method of considering the effect of the nuclear medium on the elementary branching ratios is rather simple in our model. The development of more sophisticated methods (e.g. considering the kaon self-energy) could change the value of the elementary branching ratios.

The possibilities mentioned above are either too complicated to be considered here or not yet well known, therefore they have not been included in our calculations. Their inclusion in the calculations of hypernuclear production is the goal for future studies.

Chapter 5

Conclusions

We performed calculations of the Λ-hypernuclear production within the framework of the distorted wave impulse approximation. The original formula for the capture rate containing a 3-dimensional integral was simplified using spherical coordinates, the partial wave expansion and relations for Clebsch-Gordan coefficients and spherical harmonics, to the form containing only one-dimensional integral of four wave functions.

We considered four different K^--nucleus potentials and three different pion-nucleus potentials and we found that the calculations are very sensitive to the choice of the potentials. For the considered kaon-nucleus potentials, the results for the capture rates differ up to 200%. Moreover, we conclude that the capture rates are a decreasing function of the depth of the K^--nucleus optical potential. For different pion-nucleus potentials, the results vary up to 300%. The difference between results with the free pion and the distorted pion is much larger than the difference between the results of calculations with pion distortion due to various pion-nucleus potentials.

We used a microscopic chiral model for the description of the elementary process unlike other authors who used elementary branching ratios derived ambiguously from experiment. The results for various elementary branching ratios led to the difference in the calculated capture rate of about 50%. Although the agreement with experimental

Λ-hypernuclear production rate for the elementary branching ratios derived from the microscopic model is worse than for the branching ratios derived from experiment, we prefer the former ones for theoretical reasons. Moreover, other effects influence the capture rate more than the choice of the elementary branching ratios.

The most significant effect, which was neglected in previous calculations, is the consideration of the pion distortion in the effective nucleon density available to the capture process. This quantity appears due to normalization of the capture rate for one specific process to the total capture rate, e.g. for all possible processes. We demonstrated that the change in the capture rates is up to 500%. Therefore we are convicted that the simplification adopted by previous authors is not eligible.

Finally, our results are in better agreement with experimental data than the results of previous calculations. Unfortunately, our theoretical predictions still differ from experimental data (χ^2 per data point ≈ 7), thus we still cannot be fully satisfied. We assume that there are other effects, which significantly affect the hypernuclear production capture rate, that have not been considered in our calculations.

The discrepancy between theoretical predictions and experimental data is a challenge for future studies. In addition, the experiments in FINUDA, KEK or JLab are still running and thus more experimental data are foreseen. The progress in experiment can be expected not only in the hypernuclear production induced by stopped kaon but also in the whole hypernuclear physics and in the field of the meson-baryon and meson-nucleus interaction at low and medium energies. New experimental data usually represent a challenge for theoreticians, therefore the progress in theory can be expected too.

Appendices

Appendix A

Here, we present the analytic calculation of the integral I_n from section 2.1.

$$I_n(\kappa, k_n, p_F) = \frac{\omega_n}{2\pi} \int_{\Omega_n(p_F)} \mathrm{d}^3\mathbf{l}\, \frac{1}{k_n^2 - l^2 + i\epsilon} \left(\frac{\alpha_n^2}{\alpha_n^2 + l^2} \right)^2, \tag{A.1}$$

where the integration domain is

$$\Omega_n(p_F) = \{\mathbf{l}\,;\ |\mathbf{p} + \mathbf{k_j} - \mathbf{l}| \geq p_F\}\,.$$

Let us denote the $\mathbf{p} + \mathbf{k_j} = \kappa$ and substitute the integration variable to $\mathbf{x} = \mathbf{l} - \kappa$. The integration domain then simplifies to

$$\Omega_n(p_F) = \{\mathbf{x}\,;\ |\mathbf{x}| \geq p_F\}\,.$$

We introduce spherical coordinates (r, θ, φ), where the z-axis ($\theta = 0$) lies in the direction of κ. The term l^2, which represents the only $\mathbf{l}$ dependence in the integral (A.1) is expressed as

$$l^2 = r^2 + \kappa^2 + 2r\kappa\cos\theta.$$

The integration over φ yields factor 2π. Denoting $\cos\theta = y$, we can rewrite

$$I_n = \omega_n \alpha_n^4 \int_{p_F}^{\infty} \mathrm{d}r \int_{-1}^{1} \mathrm{d}y \frac{r^2}{\left(r^2 + \alpha_n^2 + \kappa^2 + 2r\kappa y\right)^2 \left(k_n^2 - r^2 - \kappa^2 - 2r\kappa y + i\epsilon\right)}. \tag{A.2}$$

The integration over y is straightforward using the method of the partial fraction decomposition:

$$\begin{aligned} I_n = \omega_n \alpha_n^4 \int_{p_F}^{\infty} \mathrm{d}r \int_{-1}^{1} \mathrm{d}y \quad & \left(\frac{1}{(\alpha_n^2 + k_n^2)^2} \right) \frac{1}{r^2 + \alpha_n^2 + \kappa^2 + 2r\kappa y} \\ + \quad & \left(\frac{1}{(\alpha_n^2 + k_n^2)^2} \right) \frac{1}{k_n^2 - r^2 - \kappa^2 - 2r\kappa y} \\ + \quad & \left(\frac{1}{\alpha_n^2 + k_n^2} \right) \frac{1}{(r^2 + \alpha_n^2 + \kappa^2 + 2r\kappa y)^2} \,. \end{aligned}$$

The remaining integral over radius r can be expressed as a sum of three terms

$$I_n = \omega_n \left(\frac{\alpha_n^2}{\alpha_n^2 + k_n^2} \right)^2 \int_{p_F}^{\infty} \mathrm{d}r \frac{r}{2\kappa} \ln \left| \frac{\alpha_n^2 + (r+\kappa)^2}{\alpha_n^2 + (r-\kappa)^2} \right| \tag{A.3}$$

$$+\omega_n \left(\frac{\alpha_n^2}{\alpha_n^2 + k_n^2} \right)^2 \int_{p_F}^{\infty} \mathrm{d}r \frac{x}{2\kappa} \ln \left| \frac{k_n^2 - (r-\kappa)^2 + i\epsilon}{k_n^2 - (r+\kappa)^2 + i\epsilon} \right| \tag{A.4}$$

$$+\omega_n \left(\frac{\alpha_n^4}{\alpha_n^2 + k_n^2} \right) \int_{p_F}^{\infty} \mathrm{d}r \frac{2r^2}{(r^2 + \alpha_n^2 + \kappa^2)^2 - 4r^2\kappa^2} \,. \tag{A.5}$$

The expression in line (A.5) is calculated using the partial fraction decomposition:

$$\begin{aligned} (A.5) &= \omega_n \left(\frac{\alpha_n^2}{\alpha_n^2 + k_n^2} \right) \frac{\alpha_n^2}{2\kappa} \int_{p_F}^{\infty} \mathrm{d}r \left(\frac{r}{(r-\kappa)^2 + \alpha_n^2} - \frac{r}{(r+\kappa)^2 + \alpha_n^2} \right) \\ &= \omega_n \left(\frac{\alpha_n^2}{\alpha_n^2 + k_n^2} \right) \frac{\alpha_n^2}{2\kappa} \left[\frac{\kappa}{\alpha_n} \left(\arctan \left(\frac{r-\kappa}{\alpha_n} \right) + \arctan \left(\frac{r+\kappa}{\alpha_n} \right) \right) \right. \\ &\quad \left. + \frac{1}{2} \ln \left(\frac{\alpha_n^2 + (r-\kappa)^2}{\alpha_n^2 + (r+\kappa)^2} \right) \right]_{p_F}^{\infty} . \end{aligned}$$

The expressions in lines (A.4) and (A.3) are calculated using the properties of log-

arithm, the integration per partes and the partial fraction decomposition:

$$
\begin{aligned}
(A.4) \;&=\; \omega_n \left(\frac{\alpha_n^2}{\alpha_n^2+k_n^2}\right)^2 \int\limits_{p_F}^{\infty} \frac{\mathrm{d}r}{2\kappa}\Big(r\ln|r-k_n-\kappa| - r\ln|r+k_n-\kappa| \\
&\quad -r\ln|r-k_n+\kappa| - r\ln|r+k_n+\kappa| \Big) \\
&=\; \omega_n \left(\frac{\alpha_n^2}{\alpha_n^2+k_n^2}\right)^2 \Bigg[r - \alpha_n \arctan\frac{r-\kappa}{\alpha_n} - \alpha_n \arctan\frac{r+\kappa}{\alpha_n} \\
&\quad +\frac{1}{4\kappa}\left(r^2+\alpha_n^2-\kappa^2\right)\ln\frac{\alpha_n^2+(r+\kappa)^2}{\alpha_n^2+(r-\kappa)^2}\Bigg]_{p_F}^{\infty},
\end{aligned}
$$

$$
\begin{aligned}
(A.3) \;&=\; \omega_n \left(\frac{\alpha_n^2}{\alpha_n^2+k_n^2}\right)^2 \Bigg[-r + \frac{1}{4\kappa}\left((k_n+\kappa)^2-r^2\right)\ln\frac{|r+k_n+\kappa|}{|r-k_n-\kappa|} \\
&\quad +\frac{1}{4\kappa}\left((k_n-\kappa)^2-r^2\right)\ln\frac{|r-k_n+\kappa|}{|r+k_n-\kappa|}\Bigg]_{p_F}^{\infty}.
\end{aligned}
$$

The sum of the three partial results leads to the formula for I_n:

$$
\begin{aligned}
I_n \;&=\; \omega_n \left(\frac{\alpha_n^2}{\alpha_n^2+k_n^2}\right)^2 \Bigg[\frac{k_n^2-\alpha_n^2}{2\alpha_n}\arctan\frac{r-\kappa}{\alpha_n} + \frac{k_n^2-\alpha_n^2}{2\alpha_n}\arctan\frac{r+\kappa}{\alpha_n} \\
&\quad +\frac{1}{4\kappa}\left(r^2-\kappa^2-k_n^2\right)\ln\frac{\alpha_n^2+(r+\kappa)^2}{\alpha_n^2+(r-\kappa)^2} \\
&\quad +\frac{1}{4\kappa}\left((k_n+\kappa)^2-r^2\right)\ln\frac{|r+k_n+\kappa|}{|r-k_n-\kappa|} + \frac{1}{4\kappa}\left((k_n-\kappa)^2-r^2\right)\ln\frac{|r-k_n+\kappa|}{|r+k_n-\kappa|}\Bigg]_{p_F}^{\infty}.
\end{aligned}
$$

The limit at the upper bound of the integral (the infinity) of the function arctan is $\pi/2$. Since $\operatorname{arccot}(x) = \pi/2 - \arctan(x)$ we can rewrite the (upper bound − lower bound) first two terms using the function $\operatorname{arccot}(x)$.

The limit at the infinity of the remaining terms with logarithms equals zero. The introduction of the upper (the infinity) and lower (p_F) bounds then leads to the final result:

$$\begin{aligned} I_n(\kappa, k_n, p_F) &= \omega_n \left(\frac{\alpha_n^2}{\alpha_n^2 + k_n^2} \right)^2 \left[\frac{k_n^2 - \alpha_n^2}{2\alpha_n} \left(\operatorname{arccot} \frac{p_F - \kappa}{\alpha_n} + \operatorname{arccot} \frac{p_F + \kappa}{\alpha_n} \right) \right. \\ &\quad - \frac{1}{4\kappa} \left(p_F^2 - \kappa^2 - k_n^2 \right) \ln \frac{\alpha_n^2 + (p_F + \kappa)^2}{\alpha_n^2 + (p_F - \kappa)^2} \\ &\quad - \frac{1}{4\kappa} \left((k_n + \kappa)^2 - p_F^2 \right) \ln \frac{|p_F + k_n + \kappa|}{|p_F - k_n - \kappa|} \\ &\quad \left. - \frac{1}{4\kappa} \left((k_n - \kappa)^2 - p_F^2 \right) \ln \frac{|p_F - k_n + \kappa|}{|p_F + k_n - \kappa|} \right]. \end{aligned} \tag{A.6}$$

Appendix B

In this appendix, we present the evaluation of the integral in the numerator of the capture rate per hyperon (2.24). Various relations between Clebch-Gordan coefficients, 6j-symbols and spherical harmonics are taken from Varshalovich et. al [39]. The integral is

$$\mathbf{I} = \int \left\langle \left| \int \mathrm{d}^3 r \; \chi_{q_f}^{(-)^*}(\mathbf{r}) \; \rho_{if}(\mathbf{r}) \; \Psi_{NLM}(\mathbf{r}) \right|^2 \right\rangle \frac{d\Omega_{q_f}}{4\pi}. \tag{B.1}$$

It is useful to work in spherical coordinates and make use of the partial wave expansion. The wave functions of the kaon, pion and nucleon (hyperon) can be expressed (we repeat the notation from Chapter 2):

$$\Psi_{NLM}(\mathbf{r}) = R_{NL}(r) \; Y_{LM}(\Omega_r),$$

$$\chi_{q_f}^{(-)^*} = \sum_l i^{-l} \, (2l+1) \widetilde{j}_l(r) P_l(\hat{\mathbf{q}}.\hat{\mathbf{r}}),$$

$$\psi_{nljm}(\mathbf{r}) = \frac{u_{nlj}(r)}{r} \left[Y_l(\hat{\mathbf{r}}) \otimes \chi_{1/2} \right]_m^j = \frac{u_{nlj}(r)}{r} \sum_\lambda \sum_\sigma (l\lambda \, 1/2\sigma | jm) Y_{lm} \chi_{1/2\sigma}.$$

For the nucleon, it is useful to introduce

$$a_{jm} = (-1)^{j-m} \; \widetilde{a}_{j-m} \;\; , \;\; \psi_{jm}^* = (-1)^{j+m} \bar{\psi}_{j-m} \; .$$

The notation $< \cdots >$ in (B.1) denotes the sum over final states and the average over initial states. After substitution, we get

$$\begin{aligned} \mathbf{I} \;\; = \;\; & \int \mathrm{d}\Omega_{q_f} \frac{1}{2L+1} \sum_M \frac{1}{2J_i+1} \sum_{M_i} \sum_{M_f} \\ & \left| \int d^3 r \chi_q^{(-)*}(r) \Psi_{NLM} \sum_{n_Y l_Y j_Y} \sum_{n_N l_N j_N} \sum_{k,m} (-1)^{(k+m)} \right. \\ & \left. \left[\bar{\psi}_{n_Y l_Y j_Y} \otimes \psi_{n_N l_N j_N} \right]_{-m}^k < f | (a^+_{n_Y l_Y j_Y} \otimes \widetilde{a}_{n_N l_N j_N})_m^k | i > \right|^2 . \end{aligned} \tag{B.2}$$

The matrix element can be reduced in J using the Wigner-Eckhart theorem:

$$\sum_{M_i}\sum_{M_f}|<f|(a^+_{n_Yl_Yj_Y}\otimes\widetilde{a}_{n_Nl_Nj_N})^k_m|i>|^2=$$
$$\sum_{M_i}\sum_{M_f}|(-1)^{(J_f+k-J_i)}\frac{(J_iM_i\,km|J_fM_f)}{\sqrt{2J_f+1}}<f\|\hat{O}(k)\|i>|^2=$$
$$\sum_{M_i}\sum_{M_f}\frac{(J_iM_i\,J_f-M_f|km)(J_iM_i\,J_f-M_f|k'm')}{\sqrt{(2k+1)(2k'+1)}}\;\;|<f\|\hat{O}(k)\|i>|^2=$$
$$\frac{\delta_{kk'}\delta_{mm'}}{2k+1}|<f|\hat{O}(k)\|i>|^2.$$

In the following, we will omit this element for simplicity.

Now, we modify the expression for the nucleon/hyperon wave functions

$$\begin{aligned}\left[\bar{\psi}_{n_Yl_Yj_Y}\otimes\psi_{n_Nl_Nj_N}\right]^k_{-m} &= \sum_{m_Y}\sum_{m_N}(j_Ym_Y\,j_Nm_N|k-m)\bar{\psi}_{n_Yl_Yj_Ym_Y}\psi_{n_Nl_Nj_Nm_N}\\ &= \sum_{m_Ym_N}\sum_{\lambda_Y\sigma_Y}\sum_{\lambda_N\sigma_N}\frac{u^*_Yu_N}{r^2}(-1)^{(j_Y+m_Y)}Y^*_{l_Y\lambda_Y}Y_{l_N\lambda_N}\chi^+_{1/2\sigma_Y}\chi_{1/2\sigma_N}\\ &\quad (j_Ym_Y\,j_Nm_N|k-m)(l_Y\lambda_Y\,1/2\sigma_Y|j_Y-m_Y)(l_N\lambda_N\,1/2\sigma_N|j_Nm_N).\end{aligned}$$

The spin part of the wave functions gives $\delta_{\sigma_Y\sigma_N}$.

We use relations for the Clebsch-Gordan coefficients and sum over m_Y, m_N and σ_N[1]:

$$\sum_{m_Ym_N\sigma_N}(-1)^{(j_Y+m_Y)}(j_Ym_Y\,j_Nm_N|k-m)(l_Y\lambda_Y\,1/2\sigma_Y|j_Y-m_Y)(l_N\lambda_N\,1/2\sigma_N|j_Nm_N)=$$

$$(-1)^{(2j_Y-j_N+k+l_N-\lambda_Y-\lambda_N+3/2)}\sqrt{\frac{(2k+1)(2j_Y+1)(2j_N+1)}{2l_Y+1}}(kml_N\,\lambda_N|l_Y\lambda_Y)\left\{\begin{array}{ccc}j_N & j_Y & k\\ l_Y & l_N & 1/2\end{array}\right\}.$$

[1]

$$\sum_{\alpha\beta\delta}(b\beta c\gamma|a\alpha)(b\beta e\epsilon|d\delta)(a\alpha f\varphi|d\delta)=(-1)^{(b+c+d+f)}\frac{\sqrt{(2a+1)(2d+1)^2}}{\sqrt{2e+1}}\left\{\begin{array}{ccc}a & b & c\\ e & f & d\end{array}\right\}$$

The pion wave function can be written in the partial wave expansion

$$\chi_{q_f}^{(-)^*} = \sum_l i^{-l}\,(2l+1)\widetilde{j}_l(r)P_l(\hat{\mathbf{q}}.\hat{\mathbf{r}}).$$

The integration over Ω_{q_f} can be done separately, because the pion wave function is the only one, which depends on q_f

$$\begin{aligned}
&\int \mathrm{d}\Omega_{q_f} \sum_l i^{-l}(2l+1)\tilde{j}_l(r)P_l(\hat{q}\cdot\hat{r}) \sum_{l'} i^{l'}(2l'+1)\tilde{j}^*_{l'}(r')P_{l'}(\hat{q}\cdot\hat{r}') = \\
&\sum_l \sum_{l'} i^{-l+l'}(2l+1)(2l'+1)\tilde{j}_l(r)\tilde{j}^*_{l'}(r')\ \frac{4\pi}{2l+1}P_l(\hat{r}\cdot\hat{r}')\delta_{ll'} = \\
&\sum_l \tilde{j}_l(r)\tilde{j}^*_{l'}(r') \sum_\mu Y^*_{l\mu}(\hat{r})\,Y_{l\mu}(\hat{r}')\,.
\end{aligned}$$

Now, we return to equation (B.2) and put all previous expressions together

$$\begin{aligned}
\mathbf{I} \;=\; & \frac{(4\pi)^2}{(2L+1)(2J_i+1)} \sum_M \sum_{l\mu} \sum_{km} \\
& \Big[\sum_{n_Y j_Y l_Y} \sum_{n_N j_N l_N} \sum_{\lambda_Y \lambda_N} (-1)^{(2j_Y - j_N + l_N - \lambda_Y - \lambda_N + 3/2)} \\
& \sqrt{\frac{(2j_Y+1)(2j_N+1)}{2l_Y+1}} \int \mathrm{d}r\, u^*_{n_Y j_Y l_Y}(r)\, u_{n_N j_N l_N}(r)\, \tilde{j}_l(r)\, R_{NL}(r) \\
& (k m l_N \lambda_N | l_Y \lambda_Y) \begin{Bmatrix} j_N & j_Y & k \\ l_Y & l_N & 1/2 \end{Bmatrix} \int d\Omega Y^*_{l_Y\lambda_Y}(\hat{r})\, Y_{l_N\lambda_N}(\hat{r})\, Y^*_{l\mu}(\hat{r})\, Y_{LM}(\hat{r}) \Big] \Big[\ldots' \Big].
\end{aligned}$$

Here, $[\ldots']$ stands for the bracket with same relations, but with lined sum indexes and integration variables.

Let $I^l_{\gamma_Y\gamma_N}$ denote the integral over the radius r

$$I^l_{\gamma_Y\gamma_N} = \int \mathrm{d}r\, u^*_{n_Y j_Y l_Y}(r)\, u_{n_N j_N l_N}(r)\, \tilde{j}_l(r)\, R_{NL}(r).$$

After using the formula[2] for integration of four spherical harmonics, we get

$$
\begin{aligned}
\mathbf{I} \;=\; & \frac{(4\pi)^2}{(2L+1)(2J_i+1)} \sum_{M} \sum_{l\mu} \sum_{km} \\
& \Big[\sum_{n_Y j_Y l_Y} \sum_{n_N j_N l_N} \sum_{\lambda_Y \lambda_N} I^{l}_{\gamma_Y \gamma_N} (-1)^{(2j_Y - j_N + l_N - \lambda_Y - \lambda_N + 3/2)} \\
& \sqrt{\frac{(2j_Y+1)(2j_N+1)}{2l_Y+1}} (kml_N\, \lambda_N | l_Y \lambda_Y) \begin{Bmatrix} j_N & j_Y & k \\ l_Y & l_N & 1/2 \end{Bmatrix} \\
& \sum_{L_\alpha M_\alpha} \sqrt{\frac{(2l_Y+1)(2l_N+1)(2l+1)(2L+1)}{(4\pi)^2 (2L_\alpha+1)^2}} \\
& (l_Y 0\, l0 | L_\alpha 0)(l_Y \lambda_Y\, l\mu | L_\alpha M_\alpha)(l_N 0\, L0 | L_\alpha 0)(l_N \lambda_N\, LM | L_\alpha M_\alpha) \Big] \Big[\ldots' \Big].
\end{aligned}
$$

Now we modify the expression with Clebsch-Gordan coefficients:

$$
\begin{aligned}
& \sum_{\lambda_Y \lambda_N M_\alpha} (-1)^{(-\lambda_Y - \lambda_N)} (kml_N\, \lambda_N | l_Y \lambda_Y)(l_N \lambda_N\, l\mu | L_\alpha M_\alpha)(l_N \lambda_N\, LM | L_\alpha M_\alpha) = \\
& (-1)^{(L_\alpha + l + l_Y - m)} \sqrt{\frac{(2L_\alpha+1)^2 (2l_Y+1)}{(2L+1)}} (kml\mu | LM) \begin{Bmatrix} l_N & L_\alpha & L \\ l & k & l_Y \end{Bmatrix}.
\end{aligned}
$$

After substituting into previous formula and performing straightforward rearrange-

[2]

$$
\begin{aligned}
\int \mathrm{d}\Omega\, Y^*_{l_1 m_1} Y^*_{l_2 m_2} Y_{l_3 m_3} Y_{l_4 m_4} = \; & \sum_{LM} \; \sqrt{\frac{(2l_1+1)(2l_2+1)}{4\pi(2L+1}} (l_1 0\, l_2 0 | L0)(l_1 m_1\, l_2 m_2 | LM) \\
& \sqrt{\frac{(2l_3+1)(2l_4+1)}{4\pi(2L+1}} (l_3 0\, l_4 0 | L0)(l_3 m_3\, l_4 m_4 | LM)
\end{aligned}
$$

ments, we get:

$$\begin{aligned}
\mathbf{I} \;=\; & \frac{1}{(2L+1)(2J_i+1)} \sum_M \sum_{l\mu} \sum_{km} (2l+1)(km\, l\mu|LM)^2 \\
& \Big[\sum_{n_Y j_Y l_Y} \sum_{n_N j_N l_N} I^l_{\gamma_Y \gamma_N} (-1)^{(2j_Y - j_N + l_N + 3/2)} \\
& \sqrt{(2j_Y+1)(2j_N+1)(2l_N+1)} \begin{Bmatrix} j_N & j_Y & k \\ l_Y & l_N & 1/2 \end{Bmatrix} \\
& \sum_{L_\alpha} (-1)^{(L_\alpha + l_Y)} \sqrt{(2l_Y+1)} (l_Y 0\, l0|L_\alpha 0)(l_N 0\, L0|L_\alpha 0) \begin{Bmatrix} l_N & L_\alpha & L \\ l & k & l_Y \end{Bmatrix} \Big] \Big[\ldots' \Big].
\end{aligned} \tag{B.3}$$

The sum over M, m, μ gives

$$\sum_{Mm\mu} (km\, l\mu|LM)^2 = 2L+1,$$

and the sum on the last row of (B.3) can be performed explicitly

$$\sum_{L_\alpha} \ldots \;=\; (-1)^{(k)} \frac{1}{\sqrt{2l+1}} (L0\, k0|l0)(l_N 0\, k0|l_Y 0).$$

We can add any integer into the exponent of (-1), because the sign of the expression inside the brackets is irrelevant, when they are multiplied by each other. $2j_Y$ is surely odd number so we can omit it. Hence, the substitution $(-1)^{(2j_Y - j_N + l_N + 3/2)}$ by $(-1)^{(j_N + l_N + 1/2)}$ does not change the final result.

Consequently, we get

$$\begin{aligned}
\mathbf{I} \;=\; & \frac{1}{2J_i+1} \sum_{kl} (l0\, k0|L0)^2 \Big| \sum_{n_Y j_Y l_Y} \sum_{n_N j_N l_N} I^l_{\gamma_Y \gamma_N} (-1)^{(j_N + l_N + 1/2)} \\
& \sqrt{(2j_Y+1)(2j_N+1)(2l_N+1)} (l_N 0\, k0|l_Y 0) \begin{Bmatrix} j_N & j_Y & k \\ l_Y & l_N & 1/2 \end{Bmatrix} \\
& < J_f; \ldots \| \hat{O}(k) \| J_i; \ldots > \Big|^2 .
\end{aligned}$$

Now, we assume that the reaction takes place from a nucleon shell $n_N l_N$ to a hyperon shell $n_Y l_Y$ and perform the sum over all final states

$$\sum_f \frac{1}{2J_i+1} < i||\hat{O}^+(k)||f >< f||\hat{O}(k)||i > .$$

We use the relation of closure $\sum_f |f >< f| = 1$, and the definition of the reduced matrix element $< i||\hat{O}(k)||i >= (2J_i+1)\sum_m < i, m_i|\hat{O}(k,m)|i, m_i >$.

The operator $\hat{O}(k,m)$ can be expressed as the tensor sum of creation and annihilation operators:

$$\sum_m \sum_{m_Y,m_N,m'_Y,m'_N} (j_Y m_Y\, j_N m_N|km)^*\ (j'_Y m'_Y\, j'_N m'_N|km) < i|a_{j'_Y,m'_Y} a^+_{j'_N,m'_N} a^+_{j_Y,m_Y} a_{j_N,m_N}|i > .$$

Since there is no hyperon in the initial state, hyperon operators yield $\delta_{j_Y j'_Y}\ \delta_{m_Y m'_Y}$.

The sum over m, m_Y of Clebsch-Gordan coefficients gives $\delta_{m_N m'_N}\ \delta_{j_N j'_N}$ and $< i|a^+_{j_N,m_N} a_{j_N,m_N}|i >$ is a number of nucleons in a state $j_N m_N$. The sum over m_N yields the number $N(j_N)$ of nucleons in the shell j_N.

Now, we can express the integral $\mathbf{I}$:

$$\mathbf{I}_{n_N l_N \to n_Y l_Y} = \sum_{k,j_Y,j_N} (2k+1)(2l_N+1)(2j_Y+1) \left\{ \begin{array}{ccc} j_N & j_Y & k \\ l_Y & l_N & 1/2 \end{array} \right\}^2 N^{(k)}_{\gamma_Y\gamma_N} N(j_N),$$

last row where

$$N^{(k)}_{\gamma_Y\gamma_N} = \sum_l (L0\, k0|l0)^2 |I^l_{\gamma_Y\gamma_N}|^2.$$

We assume that the integrals $I^l_{\gamma_Y\gamma_N}$ are almost independent of j_Y, therefore we can sum over all j_Y. Using the relation of orthogonality for 6j-symbols[3], we finally obtain

$$\mathbf{I}_{n_N l_N \to n_Y l_Y} = \sum_k (2k+1)(l_N 0\, k0|l_Y 0) N^{(k)}_{\gamma_Y\gamma_N} N(j_N). \qquad \text{(B.4)}$$

[3] $\sum_j (2j+1)(2k+1) \left\{ \begin{array}{ccc} a & b & j \\ c & d & k \end{array} \right\} \left\{ \begin{array}{ccc} a & b & j \\ c & d & k' \end{array} \right\} = \delta_{kk'}$

Bibliography

[1] Danysz M., Pniewski J.: Phil. Mag. **44**, 348 (1953).

[2] Hashimoto O., Tamura H..: Progr. Part. Nucl. Phys. **57**, 564 (2006).

[3] Hungerford E.V. in *Topics in Strangeness Physics*, ed. P. Bydžovský, A. Gal, and J. Mareš, Lect. Notes Phys. **724**, Springer, pp. 1-29, 2007.

[4] Glendenning N.K.: Phys. Lett. B **114**, 392 (1982).

[5] Faessler M.A. et al.: Phys. Lett. B **46**, 468 (1973).

[6] Bruckner W. et al.: Phys. Lett. B **55**, 107 (1976).

[7] Bruckner W. et al.: Phys. Lett. B **62**, 481 (1976).

[8] M. Agnello et al., Phys. Lett. B **622**, 35 (2005).

[9] Milner C. et al.: Phys. Rev. Lett. **54**, 1237 (1985).

[10] Hasegawa T. et al.: Phys. Rev. Lett. **74**, 224 (1995).

[11] Hotchi H. et al.: Phys. Rev. C **64**, 044302 (2001).

[12] Miyoshi T. et al.: Phys. Rev. Lett. **90**, 232502 (2003).

[13] Friedman E., Gal A., Batty C.J.: Phys. Lett. B **308**, 6 (1993).

[14] Friedman E., Gal A., Mareš J., Cieplý A.: Phys. Rev. C **60**, 024314 (1999).

[15] Mareš J., Friedman E., Gal A.: Nucl. Phys. A **770**, 84 (2006).

[16] Brown G.E., Rho M.: Nucl. Phys. A **596**, 503 (1996).

[17] Waas T., Kaiser N., Weise W.: Phys. Lett. B **365**, 12 (1996).

[18] Cieplý A., Friedman E., Gal A., Mareš J.: Nucl. Phys. A **696**, 173 (2001).

[19] Tamura H., Hayano R.S., Outa H., Yamazaki T.: Prog. Theor. Phys. Suppl. **117**, 1 (1994).

[20] Ahmed M.W., Cui X., Empl. A., et al.: Phys. Rev. C **68**, 64004-1 (2003).

[21] Gal A., Klieb L.: Phys. Rev. C **34**, 956 (1986).

[22] Matsuyama A., Yazaki K.: Nucl. Phys. A **477**, 6 (1988).

[23] Kaiser N., Siegel P.B., Weise W.: Nucl. Phys. A **594**, 325 (1995).

[24] Oset E., Ramos A.: Nucl. Phys. A **635**, 99 (1998).

[25] Borasoy B., Nissler R., Weise W.: Eur. Phys. J. A **25**, 79 (2005).

[26] Cieplý A., Smejkal J.: Eur. Phys. J. A **34**, 237 (2007).

[27] Weinberg S.: Physica **96A**, 327 (1979).

[28] Weinberg S.: Nucl. Phys. B **363**, 3 (1991).

[29] Taylor J.R.: *Scattering theory*, John Wiley & Sons, Inc., Boulder, 1972.

[30] Rodberg L.S., Thaler R.M.: *Introduction to the Quantum Theory of Scattering*, Academic Press, Inc., New York, 1972.

[31] Van der Velde-Wilquet C. et al.: Nuovo Cimento **39A**, 537 (1977).

[32] Friedman E.: private communication with A. Cieplý

[33] Friedmann E., Gal A., Batty C.J.: Nucl. Phys. A **696**, 173 (1994).

[34] de Jager C.W., de Wries H., de Wries C.: At. Data Nucl. Data Tables **14**, 479 (1974); ibid. **36**, 495 (1987).

[35] Ericson M., Ericson T.E.O.: Ann. of Phys. **36**, 323 (1966).

[36] Thiessen H. A. et al.: LAMPF Report no. LA-7607-PR (1978).

[37] Harvey C. J. et al.: LAMPF Report no. LA-UR-84-1732 (1984).

[38] Batty C.J.: Private communication with A. Cieplý (1995).

[39] Varshalovich D.A., Moskalev A.N., Khersonskii V.K.: *Kvantovaja teorija uglovogo momenta*, Nauka, Leningrad, 1975.